Multiplexed imaging of immune cells in staged multiple sclerosis lesions by mass cytometry

Valeria Ramaglia[1*], Salma Sheikh-Mohamed[1], Karen Legg[1], Olga L Rojas[1], Stephanie Zandee[2], Fred Fu[4], Olga Ornatsky[3], Eric C Swanson[3], Alexandre Prat[2], Trevor D McKee[4] and Jennifer L Gommerman[1]

[1]Department of Immunology, University of Toronto, Toronto, Ontario, Canada.

[2]Department of Neuroscience, Faculty of Medicine, Université de Montreal, and Neuroimmunology Unit, CRCHUM, Montreal, Quebec, Canada.

[3]Fluidigm Inc., Markham Ontario

[4]STTARR Innovation center, University Health Network, Toronto, Ontario, Canada.

*Corresponding author:

v.ramaglia@utoronto.ca

Tel: +1 416-978-4119

Fax: +1 416-978-1938

Subject area: Immunology and Inflammation

Keywords: Imaging mass cytometry, multiple sclerosis, lesions, immunopathology

Acknowledgements: This work was funded by a team grant from the MS Society Research Foundation to AP and JG, and the National Multiple Sclerosis Society Research Grant RR-1602-07777 to VR.

ABSTRACT

Multiple Sclerosis (MS) is characterized by demyelinated and inflammatory lesions in the brain and spinal cord. Lesions contain immune cells with variable phenotypes and functions. Here we use imaging mass cytometry (IMC) to enable the simultaneous imaging of 15+ proteins within 11 staged MS lesions. Using this approach, we demonstrated that the majority of demyelinating macrophage-like cells in active lesions were derived from the resident microglial pool. Although $CD8^+$ T cells predominantly infiltrated the lesions, $CD4^+$ T cells were also abundant but localized closer to blood vessels. B cells with a predominant switched memory phenotype were enriched across all lesion stages and were found to preferentially infiltrate the tissue as compared to unswitched B cells which localized to the vasculature. We propose that IMC will enable a comprehensive analysis of single-cell phenotypes, their functional states and cell-cell interactions in relation to lesion morphometry and demyelinating activity in the MS brain.

INTRODUCTION

Multiple sclerosis (MS) is a disease with profound heterogeneity in the neuropathological and immunopathological appearance of lesions in the central nervous system (CNS)[28]. Recent consensus has standardized staging of MS brain tissue into categories including normal-appearing white matter (NAWM), (p)reactive lesions (or "pre-phagocytic" lesions)[3] which may represent an initial lesion[32,1], periplaque white matter (PPWM) which is immediately adjacent to a lesion, early or late active demyelinating lesions, mixed active/inactive demyelinating lesions (also called slowly expanding or "smouldering"[16]), and inactive lesions[25]. The pattern of demyelination can also be fundamentally different between patients, with pattern I being T cell-mediated, pattern II being IgG- and complement-mediated, and pattern III and IV characterized by a primary oligodendrocyte dystrophy reminiscent of virus- or toxin-induced demyelination rather than autoimmunity[15].

Lymphocytes, microglia and macrophages are associated with active demyelination and neurodegeneration in the MS brain[18,15] and are thought to play key roles in the disease process, as supported by studies in experimental models (reviewed in[36]). Depending on the type of lesion and the sub-region within a lesion (for example center vs edge), different myeloid and lymphoid cells can be found. These have a variety of phenotypes that reflect activation state and pathologic potential. With respect to myeloid cells, yolk sac-derived (resident) microglia and blood-derived (recruited) monocytes/macrophages accumulate at sites of active demyelination and neuroaxonal injury[15]. Microglia and macrophages within the MS brain can lose their normally homeostatic properties and acquire a pro-inflammatory phenotype with expression of molecules involved in phagocytosis, oxidative injury, antigen presentation and T cell co-stimulation[17]. Either via T cell-mediated

63 recognition of myelin epitopes[41] or complement binding to myelin autoantibodies[40],
64 these lymphocyte-dependent events initiate a process that results in the activation of
65 microglia and recruitment of macrophages at the lesion site. Microglia and macrophages
66 become activated and internalize myelin, degrading it within their lysosomes. The detection
67 of small (myelin oligodendrocyte glycoprotein, MOG) or large (proteolipid protein, PLP)
68 myelin proteins indicates the temporal development of myelin destruction[28,25].
69
70 In terms of lymphocytes, MS lesions contain T cells and $CD20^+$ B cells[31]. In active
71 lesions, $CD8^+$ T cells proliferate and have an activated cytotoxic phenotype. Subsequently,
72 some $CD8^+$ T cells are destroyed by apoptosis while others, with tissue-resident memory
73 features, persist. Tissue resident memory T cells lose expression of surface molecules that
74 are involved in the egress of leukocytes from inflamed tissue, which has been suggested as
75 a potential mechanism responsible for the compartmentalized inflammatory response in
76 established lesions[31]. $CD4^+$ T cells are also found in MS lesions and have been shown to
77 produce cytokines such as IL-17 and IFNγ[23]. B cells are thought to differentiate into
78 plasma cells, perhaps *in situ*, but little is known about their phenotype[31].
79
80 While past and recent immunohistological studies have provided insigths into the types of
81 immune cells populating MS lesions at different lesional stages and the neurodegenerative
82 changes that accompany these infiltrating immune cells[31,29,44,35,14,15], this type of
83 analysis requires immunohistological staining of serial sections and is limited to the number
84 of analytes that can be simultaneously visualized on a given tissue section. Thus, a
85 comprehensive analysis of single-cell phenotypes and functional states in relation to
86 demyelination within MS tissue is lacking. To circumvent this challenge, we have employed
87 imaging mass cytometry (IMC). IMC uses time-of-flight inductively coupled plasma mass

88 spectrometry to detect dozens of markers simultaneously on a single tissue section. It
89 achieves this by measuring the abundance of metal isotopes tagged to antibodies and indexed
90 against their source location[10]. Applying this new technology to post-mortem MS brain
91 tissue, we carefully analysed staged lesions in a case with severe rebound MS disease
92 activity after natalizumab (NTZ) cessation[26]. The data we collected suggests that imaging
93 mass cytometry, in combination with existing imaging techniques, can profoundly impact
94 our knowledge of the inflammatory response and tissue injury in the MS brain.

MATERIALS & METHODS

Patient case report and pathological analysis of the brain. The clinical and pathological characteristics of the case reported in this study have been previously published[26]. Briefly, the patient was a 32-year-old female, diagnosed with relapsing-remitting MS in 2005. Natalizumab (NTZ) therapy was intitiated (expanded disability status scale (EDSS) 5.0 per relapse, and 3.5 upon induction on NTZ) but stopped after 2 years because, although clinically and radiologically stable (EDSS 2.0), the patient tested positive to the John Cunningham virus (JVC) virus antibody titer. Glatiramer acetate was started 1 month prior to NTZ cessation, and the patient received a 5-day course of intravenous (iv) methylprednisolone after the last NTZ infusion. Four months later, the patient was hospitalized for the presentation of new motor and cognitive deficits. Over the course of 2 weeks, the patient worsened (EDSS 9.5). Despite daily course of iv methylprednisolone, the patient developed several new gadolinium-enhancing lesions on repeated MRI. Since no clinical or radiological improvements were observed, the family decided to stop active care, as per patient's previous wishes. Autopsy was performed within 1 hour post-mortem, 4 days after withdrawal of all medication.

The patient had previously provided written consent for post-mortem donation of the CNS to research (ethics committee approval number BH.07.001). Pathological analysis of the brain revealed abundant, active demyelinating, and highly inflammatory MS lesions with immunological pattern II (IgG- and complement-mediated)[26], according to Lucchinetti et al[28]. Despite the extent of the inflammation, progressive multifocal leukoencephalopathy or immune reconstitution inflammatory syndrome (IRIS) were excluded, from a pathological point of view, although a later study proposed that Epstein-Barr virus-associated IRIS could have been the possible cause of the fulminant MS relapse in this case[39]. Of note, immunohistochemistry and qPCR for JCV was reported negative. Finally, the neuropathologist-confirmed diagnosis of severe MS rebound inflammatory demyelinating

activity after NTZ withdrawal[26]. The non-neurological control case was an 86-year-old female that died of cardiac arrest. This control case was obtained from the Netherlands Brain Bank (VU Medical Center ethic committee approval Reference number 2009/148).

Sample characterization. Our study was performed on two frozen tissue blocks from the MS case and one frozen tissue block from the non-neurological control case. We analysed immunopathological changes in the white matter of the MS case, focusing on the following regions of interest (ROI) in lesions staged according to Kuhlmann et al[25] (see **Figure 1 – Figure Supplement 1**): normal-appearing white matter (NAWM), located > 1 cm distant from any lesions (detected in the block); the periplaque white matter (PPWM), located < 1 cm distant from any lesions; (p)reactive lesions, that may represent the initial stage of a lesion[32,1,25], defined by the presence of microglia/macrophages in the absence of (obvious) demyelination, as described by Luchetti et al[29]; early active demyelinating lesions defined by presence of microglia/macrophages with early (MOG) and late (PLP) myelin degradation products throughout the lesion, as described[7], and previously shown for this MS case[26], supporting the abundance of demyelinating activity in this type of lesions; the active edge of mixed active-inactive demyelinating lesions defined as slowly expanding lesions or smouldering lesions by Frischer et al, that are normally present in the progressive stage of MS[16] but have also been described in cases with acute MS[44]; and lastly the inactive center of a mixed active-inactive demyelinating lesion. The normal white matter of control (WMC) was analysed as a reference background for the immunopathological composition of the lesions in the MS case. The lesion types and ROI analysed are indicated in **Table 1**.

Selection of inflammatory markers. To define inflammatoty cells as a whole, we used CD45, a general marker for microglia, macrophages and lymphocytes, with $CD45^{low/+}$ indicative of

145 microglia and CD45^{high} indicative of macrophages and lymphocytes. For microglia we
146 additionally used TMEM119, that is expressed on yolk sac-derived (resident) microglia but not
147 on recruited blood-derived macrophages[5,38]. Other markers were used to detect
148 phagocytosis (CD68) and capacity for antigen presentation (human leukocyte antigen, HLA).
149 All T cells were detected with the cellular marker CD3. CD8α detected MHC class I restricted
150 T cells while CD4 detected MHC class II restricted T cells. All B cells were identified by the
151 expression of either the kappa (κ) or lambda (λ) allelic variants of the immunoglobulin light
152 chain. CD38 was used to detect a multifunctional molecule expressed by leucocytes in general
153 and involved in the activation of T cells and B cells. IgM was used to identify naïve and non-
154 class switch memory B cells, in addition to detecting free immunoglobulins. Furthermore,
155 microglia and T cells express the transcription factor nuclear factor of activated T cells
156 (NFAT1), that translocates to the nucleus upon activation[12]. Therefore, we determined the
157 localization of NFAT1 as an additional activation antigen of CD45$^{low/+}$TMEM119^{+} microglia
158 and CD45^{high}CD3^{+}CD8α^{+} or CD45^{high}CD3^{+}CD8α^{-} T cells. We also used the Ki67 marker of
159 cell proliferation and PLP to identify myelin. Blood vessels were identified using markers of
160 extracellular matrix (collagen) and endothelial cells (CD31). Each antibody clone was first
161 titrated for immunofluorescence staining in control and MS tissue, according to the dilutions
162 shown in **Table 2**, prior to methial-conjugation and IMC application.
163
164 **Histology, immunohistochemistry (IHC) and immunofluorescence (IF).** Ten-micron
165 frozen tissue sections were mounted on Superfrost Plus glass slides (Knittel Glass) and stored
166 at -80℃ until they were stained.
167
168 *Histology*. On the day of the staining, the slides were brought at room temperature and post-
169 fixed in 10% formalin for 3 hours. Tissue sections were stained with Hematoxylin and Eosin

(HE)/Luxol Fast Blue (LFB) to detect myelin lipids and Oil red O (ORO) to detect neutral lipids in phagocytic macrophages, as previously published[34].

IHC. On the day of the staining, the slides were brought to room temperature and post-fixed in ice-cold acetone for 10 minutes. Myelin protein was detected using an antibody for proteolipid protein (PLP) and microglia/macrophages were detected using an antibody for human leukocyte antigen (HLA). Endogenous peroxidases activity was blocked by incubation in PBS with 0.3% H_2O_2 for 20 minutes at room temperature. Non-specific protein binding was blocked by incubation with 10% normal goat serum (DAKO). Primary antibodies were applied overnight at 4℃, diluted in normal antibody diluent (Immunologic, Duiven, The Netherlands) according to dilutions noted in **Table 2**. The following day, sections were incubated with a post-antibody blocking solution for monoclonal antibodies (Immunologic) diluted 1:1 in PBS for 15 minutes at RT. Detection was performed by incubating tissue sections in secondary Poly-HRP (horseradish peroxidase)-goat anti-mouse/rabbit/rat IgG (Immunologic) antibodies diluted 1:1 in PBS for 30 minutes at RT followed by application of DAB (3,3-diaminobenzidine tetrahydrochloride (Vector Laboratories, Burlingame, CA, U.S.A.) as a chromogen. Counterstaining was performed with hematoxylin (Sigma-Aldrich) for 10 minutes. The sections were subsequently dehydrated through a series of ethyl alcohol solutions and then placed in xylene before being coverslipped with Entellan mounting media (Sigma Aldrich). The colorimetric staining was visualized under a light microscope (Axioscope, Zeiss), connected to a digital camera (AxioCam MRc, Zeiss) and imaged with Zen pro 2.0 imaging software (Zeiss).

IF. On the day of the staining, the slides were brought to room temperature and incubated in ice-cold acetone for 10 minutes followed by 70% ethanol for 10 minutes to reduce the

autofluorescence signal derived from the fatty myelin sheets. Slides were subsequently rehydrated in 0.05% PBS-tween for 10 minutes at room temperature followed by incubation in 10% normal goat serum (DAKO) to block nonspecific binding sites. Sections were then incubated overnight at 4℃ with primary antibody diluted in 3% normal goat serum (see dilutions in **Table 2**). Primary antibodies were detected using fluorochrome-conjugated secondary antibodies (Sigma-Aldrich) diluted 1:200 in 1% Triton-X100. Sections were incubated with DAPI (Sigma Aldrich) diluted 1:3000 to visualize the nuclei. Slides were washed in PBS, air dried and mounted in aqueous mounting medium. Using the appropriate filters, the IF signal was visualized with an Axio Imager Z1, Zeiss microscope connected to a digital camera (AxioCam 506 mono, Zeiss) and imaged with Zen pro 2.0 imaging software (Zeiss).

To control for antibodies specificity, tissue sections were stained according to the IF or IHC protocols described above except for the primary antibody incubation step, which was omitted.

Imaging mass cytometry. The work flow of imaging mass cytometry is shown in **Figure 1 – Supplement Figure 2** and explained in detail below.

Conjugation of antibodies with lanthanide metals. Lanthanide metal-conjugated antibodies were either obtained from Fluidigm (Markham, Ontario, Canada) or conjugated at SickKids-UHN Flow and Mass Cytometry Facility (Toronto, Ontario, Canada), using the MaxPar X8 labelling kit from Fluidigm (catalogue number 201169B) as previously described[19]. Briefly, a purified carrier-free antibody was partially reduced with TCEP buffer (Fluidigm, catalogue number 77720) at 37˚C. The reduced antibody was then incubated with an excess of metal-loaded MaxPar X8 polymer for 90 minutes at 37˚C. The metal-labeled antibody was then recovered using a 50kDa size exclusion filter. The percent yield of metal-conjugated antibody was determined by measuring the absorbance

of the conjugate at 280nm. The recovery of our metal-conjugated antibodies was 69-78%. Antibody stabilizer was then added to the metal-conjugated antibodies before long-term storage at 4˚C.

Staining for Imaging Mass Cytometry. On the day of staining, the slides were brought to room temperature and rehydrated with 0.05% PBS-Tween in a humidified chamber for 20 minutes at room temperature. Non-specific protein binding was blocked by incubation with 10% normal goat serum for 20 minutes at room temperature followed by incubation with blocking solution (ThermoScientific Superblock Blocking Buffer in PBS) for 45 minutes at room temperature. A cocktail of primary antibodies, diluted in 0.5% BSA, was applied overnight at 4˚C at the dilutions indicated in **Table 2**. The following day, slides were first washed with 0.05% PBS-Tween and then with PBS, followed by incubation with Iridium-conjugated intercalator (Fluidigm, catalogue number 201192B), diluted 1:2000 in 0.5% BSA for 30 minutes at room temperature. Lastly, slides were dipped in water (Invitrogen ultrapure distilled water), air dried and stored at room temperature until they were ablated.

Identification of region of interest (ROI) for laser ablation. Two serial sections each stained for either IF or IMC, were used. Based on IF staining with an antibody specific for proteolipid protein (PLP) (to visualize myelin) and DAPI (to visualize nuclei), ROIs were selected for ablation to capture the regions of interest for this study.

High-spatial resolution laser ablation of tissue sections. Tissue sections were analyzed by IMC, which couples laser ablation techniques and CyTOF mass spectrometry[2] (Cytof software v6.7). Briefly, a UV laser beam ($\lambda = 219$ nm) with a 1μmx1μm spot size is used to ablate the tissue. The laser rasters across the tissue at a rate of 200Hz (200 pixels/s) with the requisitie energy to fully remove the tissue within the selected region of interest. The ablated tissue is then carried by a stream

of inert helium and argon gas into the Helios (a CyTOF system) where the material is completely ionized in the inductively coupled plasma. The ionized material then passes through high pass ion optics to remove ions with a mass less than 75amu before the ions enter the time of flight detector where they are separated based on their mass[6,4].

Data analysis and image visualization. Images of each mass channel were reconstructed by plotting the laser shot signals in the same order they were recorded, line scan by line scan, generating pseudo-colored intensity maps of each mass channel. These data were examined using MCD Viewer (V.1.0.560, Fluidigm). For qualitative assessments, images remained at the automatic threshold generated by MCD Viewer, based on the on the 98th percentile of signal. For further analysis, data was exported from MCD Viewer as tiff files, and each channel was run through an individual analysis pipeline in CellProfiler[8,22] (V3.185) in order to despeckle the image. Composite images were created for each ROI using Image J (V1.52a), and any changes to the brightness or contrast of a given marker were consistent across ROIs.

Calculation of the limit of detection. MCD Viewer was used to export text files acquired with the Hyperion IMC instrument (Fluidigm Inc., Markham ON), which were then converted to 32-bit single-channel TIFF images. The polygon tool within ImageJ 1.15s was used to manually outline the ROI (white matter of control, normal-appearing white matter) or subROI (periplaque white matter, lesion edge, lesion core), manually identified on the bases of PLP, HLA and Iridium-intercalator signals. Grey matter was excluded from subsequent analysis. Each image was despeckled in Definiens Developer XD 2.7 (Definiens Inc, Munich, Germany), using a 2D gray-level morphological opening filter with kernel radius of 1. In addition, the intensities of each marker were normalized using a modified z score approach, in which the intensity of each pixel is divided by the sum of (mean intensity of the image plus 3 times the standard deviation of the pixels in

the image) $I_{zs} = I/(\mu_{Im}+3*\sigma_{Im})$. This normalization approach has been previously used [13] and we found that it allows for a reliable comparison between IMC markers across different channels, with per-marker comparisons holding robustly across a 16-fold antibody dilution series (data not shown).

Single-cell segmentation. In order to define cells, we used a customized segmentation algorithm that took into account both the presence of nuclear DNA Iridium-intercalator as well as a set of markers of interest (see example in **Figure 7 – Supplement Figure 1**). In brief, a Gaussian blur was applied to the DNA signal and the resulting blurred image was segmented to identify nuclear content (**Figure 7 – Supplement Figure 1a**). Segmentation around the nuclei was expanded to simulate the cytoplasm, corresponding to individual cell areas, using a combination of threshold and watershed filters (**Figure 7 – Supplement Figure 1b**). Next we interrogated the segmented image for the presence of specific markers or combinations of markers that are either biologically co-expressed, or whose expression is mutually exclusive, according to the combination of markers indicated in **Table 3**. If a nucleated cell was positive for a marker or a combination of markers (see example for CD3 in **Figure 7 – Supplement Figure 1c**), the marker(s) signal was used to refine the initial nuclear segmentation. Nucleated cells that were not positive for any of the markers used, were segmented purely based on DNA signal and expanded to simulate the cytoplasmic area around the nucleus.

Gating strategy for quantitative analysis of T cell, B cell, macrophage and microglial cell subsets. A segmented cell export of raw and normalized marker intensities for all channels in each region of interest were exported as a single csv file. The per-cell mean intensities of each marker combination, (see marker list in **Table 3**), were linearly rescaled for visualization purposes. 2D log-log biaxial scatterplots of these intensities were generated in Python (V3.6.8) using matplotlib (V3.0.3). A positive- and negative-gating strategy was applied to establish

thresholds that identify particular cell types (see **Figure 7 – Supplement Figure 2** and the method below). Quadrants were set on pathologist-verified positive cells. In brief, ROI were examined in Definiens Developer XD 2.7. Cells were manually annotated by a pathologist, based on the expression of a biologically relevant set of markers to identify cells in each class of interest as defined below. These identified positive cells were superimposed to the 2D log-log scatterplots to definitively establish gates that would capture the appropriate positivity range of each cell phenotype as shown in **Figure 7 – Supplement Figure 2**.

For T cells: All nucleated cells expressing Igκ, Igλ, IgM, CD68 and HLA were eliminated, as these markers are not expressed on T cells. Gates were established for CD3 and CD45 based on a 2D log-log scatterplot of these markers. Following the identification of T-lineage cells, the same procedure was performed for CD3 vs CD4 and CD3 vs CD8, resulting in the identification of two subpopulations: $CD4^+$ T cells and $CD8^+$ T cells. Thresholds for Ki67 (a marker of proliferation) and NFAT1 (a marker of activation) were established based on manually annotated $CD3^+KI67^+$ and $CD3^+NFAT1^+$ cells, as described above. All cell populations were validated by manual annotation as described above.

For B Cells: All nucleated cells expressing CD3, CD4, CD8 and CD68 were eliminated as these markers are not expressed on B cells. B cells were further identified by CD45 above the same threshold set for T cells. Scatterplot comparison for Igκ and Igλ intensity identified $Igκ^+$ and $Igλ^+$ single-positive populations. $Igκ^+Igλ^+$ double positive cells were eliminated as artifactual, since the two allelic variant cannot co-exist on a given cell. Within $Igκ^+$ or $Igλ^+$ B-lineage cells, we compared IgM to CD38 to determine the relative abundance of IgM^+ or $CD38^+$ cell subpopulations. All cell populations were validated by manual annotation as described above.

For macrophages and microglia: All nucleated cells expressing CD3, CD4, CD8, Igκ/λ and IgM were eliminated as these markers are not expressed on macrophages and microglia. Discrimination of the remaining cells was visualized in a scatterplot for TMEM119 and CD45.

The threshold for TMEM119 positive signal was determined by comparison to TMEM119^{+} microglial cells that were identified by manual observation, relative to other cell types. The threshold for CD45 high or low signal was determined by the comparison to manually identified TMEM^{-} macrophages. Manually identified microglial cells were used to establish the lower limit of the CD45 quadrants. Cells that were low for both TMEM119 and CD45 were labeled "other" and ignored from subsequent analysis. These latter cells, likely correspond to astrocytes, oligodendrocytes and other cell types. Both TMEM119^{+}CD45$^{low/+}$ microglial cells and TMEM^{-}CD45^{high} macrophages were further evaluated for HLA, CD68 and PLP (depicted as scatterplots), to differentiate microglia or macrophages that are either resting or activated/phagocytic/demyelinating. All cell populationes were validated by manual annotation as described above.

Generation of cell density map. The gating strategy described above was confirmed by plotting the appropriately gated cell types for major lineage markers (see examples in **Figure 7 – Supplement Figure 3**). Note that Igκ > Igλ in **Figure 7 – Supplement Figure 3a** consistent with over-representatino of κ^{+} B cells in humans[24]. Following this confirmation, the density of all relevant cell subtypes was computed within each biological region of interest. A heat map, generated using Seaborn (V0.9.0), displayed the cell counts per mm^2 of tissue.

Generation of distance map. To assess the location of identified cells relative to blood vessels, collagen^{+} perivascular regions of >10μm diameter and >800 μm^2 area were segmented, and the distance between cells of interest and the border of these perivascular regions was calculated. Similarly to the cellular density calculations, average vessel distances corresponding to the mean of the per-cell vessel distance values were computed, expressed in μm, and presented as a distance

344 heat map. Some regions did not contain any cells of a particular type, leading to undefined values
345 for those particular regions and cell type combinations (presented as "n/a", not applicable).
346
347 **Statistical analysis.** Where statistical testing was possible, all tests were performed using
348 Prism software (v5.01; GraphPadSoftware, San Diego, CA). Data distribution was tested for
349 normality. Because all variables were not normally distributed, possible correlations between
350 the density of nuclei or the density of $CD3^+$ cells (number of cells / mm^2 of tissue) detected
351 either by IF or by IMC, were investigated with the nonparametric Spearman rank correlation.
352 Differences were considered significant at $p < 0.05$.
353

RESULTS

Comparability of IF versus IMC approach and specificity of metal-conjugated antibodies on brain-resident cell types. In this study, we performed two separate IMC runs on the same patient and control tissue. The first run (Figure 1-2) was to validate our panel and the approach in general. The second run (Figure 3-7) was to evaluate the composition of immune cells across several types of lesions and sub-lesional areas. To evaluate the validity of IMC for the analysis of post-mortem MS brain tissue, we first investigated whether images generated by IMC revealed a similar number of cells expressing a given marker in a mm^2 area of tissue, as determined by IF. We used IF or IMC on serial sections from the same tissue block. Sections were stained with DAPI (IF) or Iridium-intercalator (IMC) to identify DNA in the nuclei, and with anti-CD3-FITC (IF) or anti-CD3-170Er (IMC) to identify $CD3^+$ T cells. Imaging of equivalent ROI in IF- and IMC-stained sections showed similar staining patterns with clearly resolved anatomical regions (**Figure 1a**). We also showed that IMC is able to resolve myelin engulfed by microglia/macrophages with a similar pattern as what is observed using IHC and IF approaches (**Figure 1 – Supplement Figure 3**). Quantification analysis showed that the number of nuclei or $CD3^+$ T cells detected by IMC is on average 1.4 and 1.5 fold higher than numbers detected by IF, respectively. The increase in detection of cell counts across ROI for DNA and for CD3 using the IMC method compared to IF is either due to the necessary use of a serial section for comparison between the two techniques, or alternatively IMC may be a more sensitive approach for detecting nucleated cells within brain tissue. We also compared the number of nuclei identified with DAPI by IF and the number of nuclei identified with intercalator by IMC, as well as the number of $CD3^+$ T cells identified with FITC-labeled secondary antibody by IF and the number of $CD3^+$ T cells identified with the 170Er metal-tag by IMC. Both comparisons revealed a significant positive correlation (Spearman correlation coefficient: $r=0.9182$, $p=0.0002$ and $r=0.8929$, $p=0.01$, for nuclei and for $CD3^+$ T cells

379 respectively) (**Figure 1b, c**), indicating proportional representation of brain-resident cells was
380 in agreement for both methods. Collectively, IMC reproduces staining patterns that are in
381 agreement with those produced using a standard IF method in MS brain tissue.
382
383 Second we assessed the target specificity of metal-tagged antibodies by IMC. We stained brain
384 tissue with metal-tagged antibodies against molecules that are either expected to be co-
385 expressed by cells or whose cellular expression is expected to be mutually exclusive. IMC
386 imaging of the edge of an active demyelinating lesion identified $CD3^+CD45^+$ T cells and $CD3^-$
387 $CD45^+$ leukocytes other than T cells (**Figure 2a**). The co-expression of CD68 in the latter cell
388 types identifies these as microglia/macrophages ($CD3^-CD45^+CD68^+$) (**Figure 2b**). As
389 expected, $CD3^+$ T cells lack expression of immunoglobulin light chain, ($CD3^+\kappa/\lambda^-$). Since
390 antibodies directed to the B cell-restricted lineage markers CD19 and CD20 were sub-optimal
391 on our brain tissues, we relied instead on antibodies that detect the two allelic variants of the
392 immunoglobulin light chain (κ/λ). This provided two advantages: the ability to capture all B
393 cells, irrespective of their maturation/activation status (for example, plasma cells downregulate
394 CD19/CD20) and the ability to test specificity of our B cell directed reagents since κ and λ are
395 allelically excluded on the surface of B cells. As expected, we identified B cells that were either
396 positive for the κ or the λ light chain of immunoglobulins and negative for the CD3 marker of
397 T cells and the CD68 marker of macrophages (for example, $CD3^-CD68^-\kappa^+$ B cells in **Figure 2c**
398 **arrow**, versus $CD3^-CD68^-\lambda^-$ B cells in **Figure 2d arrow** and vice versa $CD3^-CD68^-\kappa^-$ B cells
399 in **Figure 2c arrow head**, versus $CD3^-CD68^-\lambda^+$ B cells in **Figure 2d arrow head**). We found
400 that the extracellular matrix protein collagen (not cell-associated) surrounded putative blood
401 vessels lined by endothelial cells that expressed the CD31 marker as expected. In contrast,
402 macrophages visualized by CD68 do not stain positive for collagen nor express CD31 ($CD31^-$
403 $collagen^-CD68^+$) (**Figure 2e**). Lastly, we asked whether the IMC approach would have

404 sufficient sensitivity to detect soluble molecules that can be rare in tissues. For this, we used
405 an antibody against granzyme B, a serine protease with pro-inflammatory function produced
406 by activated cytotoxic T cells. IMC identified a granzyme B^+ signal with granular expression
407 in close proximity to nuclei (**Figure 2f, g**). These results show that IMC enables imaging of
408 multiple markers on a single tissue section reproducing IF-equivalent staining patterns and with
409 cell lineage-specific markers expressed on appropriate cell types.
410
411 **Qualitative staging of MS lesions by IMC.** To verify whether IMC provides us with the
412 ability to differentiate normal-appearing tissue versus different lesional stages of the MS brain,
413 we analysed the proteolipid protein (PLP) signal that visualizes myelin and the human
414 leukocyte antigen (HLA) signal that visualizes antigen presenting cells (**Figure 3**). Note that
415 in some ROI, the PLP staining pattern reflects the cross-sectional orientation of myelinated
416 fibers (for example WMC and NAWM), whereas in others, longitudinal myelin tracks are
417 observed (for example (p)reactive). The different orientation of the tissue results from the
418 sectioning plane of the tissue block and is reflected in the staining pattern displayed. Consistent
419 with the generally non-inflamed and myelinated state of healthy white matter, control white
420 matter showed intact myelin staining with few HLA^+ cells (**Figure 3 a, b**). Normal appearing
421 white matter (NAWM) in the MS brain exhibited normal myelin staining, however HLA^+ cells
422 within the MS NAWM appeared enriched when compared to control white matter (**Figure 3 c,**
423 **d**). Similarly, the (p)reactive lesion showed a normal myelin signal but HLA^+ cells accumulated
424 at this site (**Figure 3 e, f**). The active lesion core showed loss of PLP signal with accumulation
425 of HLA^+ cells (**Figure 3 g, h**). The mixed active-inactive lesions showed reduced myelin and
426 accumulation of HLA^+ cells at the lesion edge (**Figure 3 i, j**). HLA^+ cells that contained PLP
427 myelin products were found in both active lesions[26] (**Figure 3k**) and at the edge of mixed
428 active-inactive lesions (**Figure 3l**), indicative of demyelinating activity. Collectively we were

able to show that IMC of different ROI (pre-selected on the bases of PLP/HLA IF staining on a serial section) was able to differentiate between normal-appearing tissue and different lesional stages of the MS brain.

Qualitative assessment of microglia and macrophages in staged MS lesions by IMC. Next, we analysed key molecules that differentiate between the phenotype and functional status of microglia and macrophages in relation to the lesional stage and demyelinating activity of MS lesions.

Control subject white matter. In the white matter from a control subject we found that microglia, identified as being $TMEM119^+$, generally showed a thin ramified morphology, typical of resting cells (**Figure 4 a, a' dotted arrows**). On these cells, the HLA marker of antigen presentation was generally low or not detectable, confirming a quiescent state. On the contrary, $TMEM119^+$ microglia that showed a more rounded morphology, which is a sign of activation, also stained for HLA and CD68 (**Figure 4 a, a' arrow head and b, b' arrow head**). HLA/CD68 expression is indicative of antigen presentation and phagocytic activity, respectively. $TMEM119^-HLA^+CD68^+$ cells were identified as macrophages and were also present in the white matter of control (**Figure 4 a, a' arrow and b, b' arrow**). These data indicate that in the normal white matter of a control subject some microglia ($TMEM119^+$) and some macrophages ($TMEM119^-$) have an activated phenotype (HLA^+CD68^+).

Normal-appearing white matter. Visualization of the expression pattern of microglia and macrophage markers in the normal-appearing white matter showed some $TMEM119^+$ microglia with ramified morphology (**Figure 4 c, c' dotted arrows**), similar to control white matter. However unlike control white matter, the normal-appearing white matter showed many $TMEM119^+$ microglia that were also positive for HLA and CD68 (**Figure 4 c, c' arrows head**

453 **and d, d' arrows head**). A few TMEM119^{-}HLA^{+}CD68^{+} macrophages were also present in the
454 normal-appearing tissue (**Figure 4 c, c' arrow and d, d' arrow**).
455 *(P)reactive lesions.* Within the (p)reactive lesions, TMEM119^{+} microglia accumulated,
456 showed an enlarged morphology that is indicative of an activated state, and expressed both
457 HLA and CD68 (**Figure 4 e, e' and e'' arrows head and f, f' arrows head**). TMEM119^{-}
458 HLA^{+}CD68^{+} macrophages were also present (**Figure 4 e, e' arrows and f, f' arrows**).
459 *Active lesions.* Active lesions contained high numbers of TMEM119^{+}HLA^{+}CD68^{+} microglia
460 and TMEM119^{-}HLA^{+}CD68^{+} macrophages, most of them with enlarged and foamy
461 morphology that is typical of the activated and phagocytic state (**Figure 4 g, g' and g'' arrows**
462 **and h, h' arrows**).
463 *Mixed active-inactive lesion (slowly expanding lesion).* The edge of these lesions was
464 characterized by a rim of dense TMEM119^{+}HLA^{+} microglia (**Figure 4 i, i' arrow head and j,**
465 **j' arrow head**) and TMEM119^{-}HLA^{+} macrophages (**Figure 4 i, i' arrows and j, j', j''**
466 **arrows**), both with obvious enlarged CD68^{+} lysosomes (**Figure 4 j'' arrows**). Only a few
467 HLA^{+}CD68^{+} cells were present in the inactive lesion core and microglia showed profound
468 reduction in the HLA signal (**Figure 4 i, i' arrows and j, j', j'' arrows**).
469
470 **Qualitative assessment of T cells in staged MS lesions by IMC.** Next, we analysed key
471 molecules that differentiate between the phenotype and functional status of T cells in relation
472 to the lesional stage and demyelinating activity of MS lesions.
473 *Control subject white matter.* In the white matter from a control subject CD3^{+}CD8α^{-} T cells or
474 CD3^{+}CD8α^{+} T cells were rare of absent (**Figure 5 a, a' and b, b'**).
475 *Normal-appearing white matter.* In the normal-appearing white matter, we identified some
476 CD3^{+}CD8α^{-} T cells (**Figure 5 c, c' arrow**) and some CD3^{+}CD8α^{+} T cells (**Figure 5 c, c'**
477 **dotted arrow**) that did not show signs of activation as defined by the expression of NFAT1

478 which translocates to the nucleus of T cells upon T cell receptor activation[30] (**Figure 5 d, d'**
479 **arrow and dotted arrow**).
480 *(P)reactive lesions.* Within the (p)reactive lesions, $CD3^+CD8\alpha^-$ and $CD3^+CD8\alpha^+$ T cells were
481 both prominent (**Figure 5 e, e' arrow and dotted arrow, respectively**) but did not stain for
482 NFAT1 and were therefore presumably not activated (**Figure 5 f, f' arrow and dotted arrow,**
483 **respectively**).
484 *Active lesions.* Active lesions contained both, $CD3^+CD8\alpha^-$ and $CD3^+CD8\alpha^+$ T cells (**Figure 5**
485 **g, g' arrow and dotted arrow, respectively**), mostly located in the perivascular area (**Figure**
486 **5 g' inset)**, but also scattered in the parenchyma. Some $CD3^+CD8\alpha^+$ T cells were also activated
487 based on the expression of NFAT1 (**Figure 5 h, h' arrow head**).
488 *Mixed active-inactive lesion (slowly expanding lesion).* Similar to the core of active lesions,
489 the edge of the slowly expanding lesions contained both, $CD3^+CD8\alpha^-$ and $CD3^+CD8\alpha^+$ T cells
490 (**Figure 5 i, i' arrow and dotted arrow, respectively**). A few $CD3^+CD8\alpha^-$ T cells and some
491 $CD3^+CD8\alpha^+$ T cells were also $NFAT1^+$ (**Figure 5 j, j' white arrow and yellow arrow head,**
492 **respectively**). These were found both in the perivascular area and in the parenchyma (**Figure**
493 **5 j'')**. The staining pattern of NFAT1 was consistent with the nuclear localization of this
494 transcription factor (**Figure 5 k-n)**. Nuclear NFAT1 signal was also observed on $CD3^-$ cells,
495 consistent with reports of its localization of cells other than T cells[30] (**Figure 5 h, h' and j,**
496 **j' white arrows head)**. Occasionally, we observed $Ki67^+$ proliferating cells (**Figure 5 o,**
497 **arrow and inset)**, some of which were $CD3^+$ T cells (**Figure 5 o, dotted arrow)**. In the inactive
498 lesion core, we observed both scattered $CD3^+CD8\alpha^-$ T cells and $CD3^+CD8\alpha^+$ T cells **(Figure 5**
499 **i**).
500

Qualitative assessment of B cells in staged MS lesions by IMC. Next we analysed key molecules that differentiate between the phenotype and functional status of B cells in relation to the lesional stage and demyelinating activity of MS lesions.

Control subject white matter. IgM staining on cells can be indicative of either naive B lymphocytes or IgM memory B cells. Therefore we first analysed the tissue for the presence of cell-associated IgM staining signal. In control white matter, IgM was not found in association with cells in the parenchyma but was only found in association with blood vessels, identified by the collagen staining. Further analysis showed that the IgM signal in the perivascular space co-localizes with the immunoglobulin light chain Igκ/Igλ, indicating that this IgM^+ $Igκ/Igλ^+$ signal represents either naive or IgM memory B cells, or alternatively cell-free immunoglobulins (**Figure 6 a, a' and b, b' arrow head**).

Normal-appearing white matter. In the normal-appearing white matter, the IgM signal was found both in association with blood vessels (**Figure 6 a, a' and b, b' arrow head**) and with nucleated $Igκ/Igλ^+$ B cells scattered in the parenchyma (**Figure 6 a, a' and b, b' dotted arrows**). Nucleated $Igκ/Igλ^+$ B cells that were IgM^- were also found in the parenchyma (**Figure 6 a, a' and b, b' solid arrows**) indicating the presence of class switched B cells.

(P)reactive lesions. Within the (p)reactive lesions, IgM was exclusively detected witin blood vessels (**Figure 6 e, e' arrow head**). Nucleated $Igκ/Igλ^+$ B cells were present and expressed a switched B cell phenotype (IgM^-) (**Figure 6 e, e' and f, f' solid arrows**).

Active lesions. Within the active lesions, nucleated $Igκ/Igλ^+$ B cells that displayed a switched phenotype (IgM^-) were mostly present (**Figure 6 g, g' and h, h' solid arrows**).

Mixed active-inactive lesion (slowly expanding lesion). Similarly to active lesions, at the edge of mixed active-inactive lesions, nucleated $Igκ/Igλ^+$ B cells were present and displayed a switched memory phenotype (IgM^-) (**Figure 6 i, i' and j, j' solid arrows**).

15-plex quantification of immune cells in staged MS lesions by IMC. Following the visualization of markers of interest in tissue sections by IMC, we pre-set thresholds for each marker and analysed combinations of markers that identify the phenotype and functional status of immune cells, as shown in **Figure 7 – Supplement Figure 2**. Focusing on the MS tissue, we assembled these data into heat maps to visualize quantitatively the cellular content of each region of interest (**Figure 7a**).

Macrophages and microglia. $CD45^{high}HLA^{+}TMEM^{-}$ macrophages were found in the normal-appearing white matter and a low density of macrophages (3 cells/mm^2) contained PLP within their $CD68^{+}$ lysosomes, indicative of demyelinating activity. The number of demyelinating $CD45^{high}HLA^{+}TMEM^{-}CD68^{+}PLP^{+}$ macrophages drastically increased in the (p)reactive lesions (34.8 cells/mm^2), reaching peak density in the core of active lesions (36.5 cell/mm^2) and edge of active-inactive demyelinating lesions (50.5 cell/mm^2). In the active core we also found a high density (92.6 cell/mm^2) of $CD45^{high}HLA^{+}TMEM^{-}CD68^{+}PLP^{-}$ macrophages, which represent phagocytes with enlarged but empty vacuoles.

Similarly to demyelinating $CD45^{high}HLA^{+}TMEM^{-}CD68^{+}PLP^{+}$ macrophages, demyelinating $CD45^{low}HLA^{+}TMEM^{+}CD68^{+}PLP^{+}$ microglia were found in high numbers in the (p)reactive lesions with peak density in the core of active lesions (249.5 cell/mm^2) and edge of active-inactive demyelinating lesions (403.3 cell/mm^2). Also in line with the distribution of non-demyelinating macrophages, a high density (224.9 cell/mm^2) of non-demyelianting $CD45^{low}HLA^{+}TMEM^{+}CD68^{+}PLP^{-}$ microglia with empty vacuoles were found in the core of active lesions. Overall, we found that in the core of active lesions on average 79% of HLA^{+} cells are microglia and that they constitute 87% of the actively demyelinating (PLP^{+}) phagocytes. In the edge of a mixed active-inactive demyelinating lesion, we found that on average 88% of HLA^{+} cells are microglia and that they constitute 89% of actively demyelinating (PLP^{+}) phagocytes.

551 *T cells.* Both $CD45^{high}CD3^{+}CD8\alpha^{+}CD4^{-}$ (CD8) T cells and $CD45^{high}CD3^{+}CD8\alpha^{-}CD4^{+}$ (CD4)
552 T cells were abundant in the MS tissue from the (p)reactive lesional stage (CD8, 53.4
553 cells/mm^2, CD4, 49.7 cells/mm^2) with peak densities in the core of active lesions (CD8, 58.6
554 cells/mm^2, CD4, 38.5 cells/mm^2), the periplaque (CD8, 92.3 cells/mm^2, CD4, 32.2 cells/mm^2)
555 and the rim (CD8, 43.2 cells/mm^2, CD4, 68.8 cells/mm^2) of mixed active-inactive lesions.
556 Overall, we found that in the core of active lesions on average 60% of T cells are $CD8^{+}$, 3% of
557 which are activated and proliferating ($NFAT^{+}Ki67^{+}$). On the contrary, in the edge of a mixed
558 active-inactive lesion, we found that on average 61% of T cells are $CD4^{+}$, 17% of which are
559 activated and proliferating ($NFAT^{+}Ki67^{+}$). We verified these findings by examining an
560 independent combination of markers – co-expression of CD38 and HLA on both CD4+ and
561 CD8+ T cells is associated with T cell activation in the context of viral infection[43]. We found
562 that $CD4^{+}CD38^{+}HLA^{+}$ and $CD8^{+}CD38^{+}HLA^{+}$ were likewise enriched in the core of the active
563 lesion and the edge of the active/inactive lesion with $CD4^{+}CD38^{+}HLA^{+}$ T cells being
564 particularly represented at the edge of the active/inactive lesion. However unlike the
565 $NFAT^{+}Ki67^{+}$ T cells, $CD38^{+}HLA^{+}$ T cells were present in particularly high density in the
566 (p)reactive lesion.
567 *B cells.* Using the CD38 marker, we were able to further define B cells sub-populations beyond
568 the qualitative images in **Figure 6**. We found B cells across all lesion types with switched
569 memory $CD45^{high}Ig\kappa/Ig\lambda^{+}IgM^{-}CD38^{+}$ B cells predominating in the core of active lesions (29.2
570 cells/mm^2, 58% of all detected B cells) and periplaque white matter (22.2 cells/mm^2, 87% of
571 all detected B cells) and at the lesion rim (44.0 cells/mm^2, 44% of all detected B cells) of
572 mixed active inactive lesions.
573
574 **Analysis of the distribution of immune cells in staged MS lesions by IMC.** Since the
575 distribution of blood-derived immune cells in relation to blood vessels can inform on the

relationship between immune infiltrates and tissue injury, we performed a morphometric analysis of the distance between functional cell types and blood vessels in different MS lesion areas (**Figure 7b**).

Macrophages. We found that demyelinating $CD45^{high}HLA^{+}TMEM^{-}CD68^{+}PLP^{+}$ macrophages infiltrated the lesion parenchyma in (p)reactive lesions (average distance from blood vessels, 136µm) and periplaque white matter (average distance from blood vessels, 131-191µm), indicating that demyelinating events occur already in tissue that does not show obvious signs of demyelination. Demyelinating macrophages were mostly found in close proximity to blood vessels in active demyelinating lesions (average distance from blood vessels, 87µm) and at the edge of active-inactive demyelinating lesions (average distance from blood vessels, 70µm). Non-demyelinating $CD45^{high}HLA^{+}TMEM^{-}CD68^{+}PLP^{-}$ macrophages were found within the lesion parenchyma in both active lesions (average distance from blood vessels, 107µm) and active-inactive lesions (edge: average distance from blood vessels, 244µm; core:average distance from blood vessels, 279µm), representing phagocytes that are no longer actively demyelinating.

T cells. In (p)reactive and periplaque white matter, both $CD8^{+}$ and $CD4^{+}$ T cells infiltrated the parenchyma ($CD8^{+}$ T cells: average distance from blood vessels, 114-238µm; $CD4^{+}$ T cells: average distance from blood vessels, 80-208µm). At the edge ($CD8^{+}$ T cells: average distance from blood vessels, 45µm; $CD4^{+}$ T cells: average distance from blood vessels, 21µm) and core ($CD8^{+}$ T cells: average distance from blood vessels, 121µm; $CD4^{+}$ T cells: average distance from blood vessels, 89µm) of active-inactive lesions, $CD4^{+}$ T cells were located in closer proximity to blood vessels compared to $CD8^{+}$ cells, which instead appeared to diffusely infiltrate the lesional parenchyma. $CD8^{+}$ and $CD4^{+}$ T cells were found to equally infiltrate the

599 parenchyma in active lesions ($CD8^+$ T cells: average distance from blood vessels, 89μm; $CD4^+$
600 T cells: average distance from blood vessels, 88μm).
601 *B cells.* We found that naïve $CD45^{high}Ig\kappa/Ig\lambda^+IgM^+CD38^-$ B cells and switched memory
602 $CD45^{high}Ig\kappa/Ig\lambda^+IgM^-CD38^+$ B cells infiltrated the parenchyma in both (p)reactive lesions
603 (naïve B cells: average distance from blood vessels, 62μm; memory switched B cells: average
604 distance from blood vessels, 92μm) and periplaque white matter (naïve B cells: average
605 distance from blood vessels, 71μm; memory switched B cells: average distance from blood
606 vessels, 103-113μm). Within lesions, naïve B cells were focally located in the perivascular
607 space of veins at the the edge (average distance from blood vessels, 2μm) and core (average
608 distance from blood vessels, 9μm) of active-inactive lesions. Switched memory
609 $CD45^{high}Ig\kappa/Ig\lambda^+IgM^-CD38^+$ B cells were present in the vicinity of blood vessels at the rim
610 (average distance from blood vessels, 44μm) and core (average distance from blood vessels,
611 19μm) of active-inactive lesions but were found to also diffusely infiltrate the parenchyma of
612 active lesions (average distance from blood vessels, 82μm).

DISCUSSION

In this study we used imaging mass cytometry to multiplex 15+ markers to stain a single tissue section. The panel contained both cell-specific and functional markers, and enabled the analysis of single-cell phenotypes and functional states of resident microglia, blood-derived (recruited) macrophages, T and B lymphocytes in demyelinating and highly inflammatory lesions in a case of severe rebound MS disease activity after natalizumab cessation[26]. We first showed the validity of the technology on post-mortem MS brain tissue and then applied it to the analysis of immune cells in the lesions compared to control brain tissue.

IMC reproduced IHC- and IF-equivalent staining patterns with no apparent changes in specificity compared to standard IF. Therefore, antibodies validated with IF for the study of the MS brain will likely be applicable to the IMC approach. It should be noted, however, that the concentration and the staining conditions of some IHC- or IF-verified antibodies may not be implemented as is into the IMC protocol: titration and/or amplification (for example with biotin-streptavin) of pathologist-verified antibodies is required for optimal visualization by IMC.

In addition to visualizing a multitude of cell types, IMC allows for inclusion and exclusion criteria of selected markers to provide better confidence of cell identity. Furthermore, the highly quantitative nature of the IMC approach enables the analyses of data with pre-set thresholds for each marker, and permits further validation based on combination (inclusion/exclusion) with other markers. For example, we were able to distinguish $CD45^{high}$ cells that were $TMEM119^{-}CD68^{+}$ thus identifying macrophages *versus* $CD45^{low/+}$ cells that were $TMEM119^{+}CD68^{+}$ thus identifying microglia.

We found that in the control brain, microglial cells lose their homeostatic phenotype and acquire an activated state. This is in line with an earlier study demonstrating expression of certain activation markers by microglia within the normal human brain, and it is in agreement with recent immunohistological findings that show no expression of the homeostatic molecule P2RY12[42] in 48% of microglia in control brains[44]. Whether this activation state is the result of systemic exposure to recurrent infections[33] or is the result of vascular and neurodegenerative changes related to normal ageing[11] (the control subject was 86 years), or whether it is an inherent property of microglia in the human brain[44], is unclear.

In line with recent observations in carefully staged lesions from a large cohort of MS patients at well-defined disease stages[44], we found that microglial activation was not restricted to lesional tissue but was also present in the normal-appearing white matter and (p)reactive lesion site. In these regions, although myelination appeared normal, we also found that demyelinating blood-derived macrophages infiltrated the parenchyma. In active lesions and in the active edge of mixed active-inactive demyelinating lesions[25] (slowly expanding or 'smouldering'[15]), microglia and macrophages displayed similar phenotypic changes characterized by the predominant expression of markers associated with activation and phagocytosis. In contrast, in the core of mixed active-inactive demyelinating lesions, microglia and macrophages lost expression of molecules involved in antigen presentation and drastically reduced their phagocytic activity, as previously described[44]. Notably, a large proportion (on average 88%) of demyelinating macrophage-like cells in active lesions and at the edge of mixed active-inactive lesions were derived from the resident microglial pool, whereas macrophages that infiltrated the parenchyma of these lesional areas were largely inactive as indicated by the presence of enlarged but empty vacuoles in these cells. This is likely the result

662 of the macrophage's inability to digest the myelin's neutral lipid components that accumulate
663 and persist in macrophages.
664
665 In terms of lymphocytes, in classical active lesions and mixed active-inactive demyelinating
666 lesions we showed that T cells were abundant. Although $CD8^+$ T cells generally predominated
667 across lesional stages, and in some cases proliferated (as also shown in a recent study[31]),
668 interestingly we found a conspicuous number of $CD4^+$ T cells not only within lesions but also
669 at the (p)reactive lesion site and periplaque white matter. In addition, $CD4^+CD38^+HLA^+$
670 "chronically activated" T cells[43] were also particularly abundant in the (p)reactive lesion
671 site. This suggests an involvement of these cells in the early stages of lesion formation, even
672 in established lesions. Similar to other findings in the case of T lymphocytes, our data also
673 reproduced immunohistological findings that described B lymphocytes in all lesion stages in
674 lower numbers compared to T cells [31]. By using IgM in combination with CD38 and κ/λ,
675 our panel has the increased capacity of identifying different B cell subsets . Indeed, by using
676 IgM in combination with CD38 and κ/λ, our panel has revealed different B cell subsets,
677 including IgM^+ and switched memory B cells.
678
679 With the IMC approach, we were able to reproduce findings by Machado-Santos et al wherein
680 they proposed that although active demyelination is associated with activated blood-derived
681 macrophages, it is largely driven by the resident activated microglial pool[44]. This was also
682 suggested by earlier studies[27], pointing to the possibility that therapeutic intervetions aimed
683 at blocking entry of myeloid cells from the circulation into the brain parenchyma may be
684 insufficient to halt the disease process.
685

686 It has been suggested that $CD8^+$ T cells in lesions from patients with relapsing, progressive and
687 fulminant acute MS show features of tissue-resident memory cells and play a central role in
688 the establishment of tissue-specific immunological memory, propagating chronic
689 compartmentalized inflammation and tissue damage in the MS brain by local activation
690 following re-exposure to their cognate antigen[31]. B cells are also detected in all MS lesion
691 types but their localization seems to be restricted to the pervascular space of some veins[31].
692 Machado-Santos et al have shown that the majority of B and T cells are present in the
693 perivascular cuffs, distant from sites of initial myelin damage[31]. This supports the possibility
694 that demyelination is induced by soluble factors produced by lymphocyte which diffuse into
695 the tissue and in turn activate phagocytes. Our findings from a single MS case with high
696 inflammatory activity only incompletely reproduce these findings. While we also observed
697 perivascular localization of B and T cells, these lymphocytes were also found to diffusely
698 infiltrate the lesion parenchyma, which could support a contact-mediated active demyelination,
699 at least in this MS case. However, due to the nature of the acquired region of interest, which
700 doesn't capture the areas surrounding the site of ablation, it is possible that blood vessels were
701 positioned immediately outside the region of interest. These would be missed in the cell-blood
702 vessel distance analysis, which would result in considering cells that may in reality have a
703 perivascular localization, as been located far from blood vessels. Further analysis of larger
704 areas across multiple tissue samples are required to better answer this question.
705
706 A comprehensive phenotypic characterization of B cells in MS tissue is lacking and the role of
707 B cells in MS lesions is currently unresolved. Recent clinical studies have reported a protective
708 effect of therapies targeting $CD20^+$ B cells in MS patients, suggesting a major role for B cells
709 in the disease process[20,21]. Our IMC results allowed for better segregation of B cell
710 phenotypes (memory, class switched etc). Further addition of other markers, particularly for

711 plasma cells (such as CD138, TACI) will be important for a full characterization of B cell
712 subsets within the MS brain. This is particularly relevant in light of recent findings that
713 demonstrate that some B lineage cells play a protective role in neuroinflammatory
714 processes[37].
715
716 While IMC has the advantage of multiplexing capability, it also has limitations. For example,
717 it yields information only about the brain region imaged and is low throughput. It is therefore
718 possible that different cell populations can exist in brain regions and sublesional areas other
719 than those imaged. As is the case for the analysis of tissue stained with standard IHC/IF
720 methods, multiple regions must be acquired. Another limitation, that seems apparent from the
721 tissue that we examined, is that cell densities by IMC were higher than those derived by IF
722 (**Figure 1**). This may be due to the fact that we had to use a serial section to compare the two
723 methods, with the two sections containing slightly different numbers of cells. Alternatively,
724 IMC may have an increased sensitivity in brain tissue compared to IF. However, in spite of
725 these differences, the proportionality of the output signal for IMC vs IF was consistent across
726 samples (Figure 1 and [9]). In addition, our study has the limitation that it is based on the
727 analysis of immune cells in lesions from a single MS. Our goal was not to uncover novel cell
728 populations in the MS brain, but rather to provide proof that the IMC technology can be used
729 as a powerful tool for the analysis of complex cellular phenotypes in heterogeneous tissues
730 such as the MS brain. Moreover, given that the cells in these lesions had known phenotypes,
731 the supervised approach for thresholding used herein was reasonable. However in the future,
732 unsupervised analysis of data sets generated using the IMC approach may identify novel cell
733 types in tissue that is understudied, for example the MS meninges. In addition, discovery of
734 novel cell types using a technique such as IMC can then be recapitulated with standard
735 techniques using multiple well-characterized specimens from established brain banks.

736

737 Overall, our data reproduced immunohistological patterns of microglia and lymphocytes
738 activation described in carefully staged MS brain lesions at well-defined disease stages[31,44]
739 using a multi-parameter approach. The significance of observed B cells of IgM memory and
740 class switch memory phenotypes, warrant further study. We propose that IMC will enable a
741 high dimentional analysis of single-cell phenotypes along with their functional states, as
742 well as cell-cell interactions in relation to lesion morphometry and (demyelinating) activity.
743 The IMC approach in combination with exhisting imaging techniques, can profoundly
744 impact our knowledge of the nature of the inflammatory response and tissue injury in the
745 multiple sclerosis brain.

746

747 **Acknowledgements.** We would like to thank the brain donors.

748

749 **Competing interest.** J.L.G. is a consultant for Roche (Canada) and currently holds grants
750 with Novartis, EMD Serono, and Roche. V.R. received a consulting honorarium from
751 EMD Serono. O.O. and E.C.S. are employees of Fluidigm Inc. The remaing authors declare
752 no competing interest**.**

753

754 **Author contributions.** V.R. performed the pathological characterization for the MS lesions,
755 guided the acquisition of the IMC data and contributed to data analysis. S.S.M. performed the
756 IF and IMC staining, and contributed to the data analysis. K.L. contributed to the optimization
757 of the IMC staining. O.L.R and V.R. supervised the optimization of the IMC staining. S.Z.
758 performed the histological staining. A.P. acquired the patient tissue. Both A.P. and O.O.
759 contributed intellectually. E.S. acquired the IMC data. T.D.M. and F.F. analysed the data.

760 J.L.G. supervised the study. V.R and J.L.G. contributed to the design of the study and wrote
761 the manuscript.

References

1. Alvarez JI, Saint-Laurent O, Godschalk A, Terouz S, Briels C, Larouche S, Bourbonniere L, Larochelle C, Prat A (2015) Focal disturbances in the blood-brain barrier are associated with formation of neuroinflammatory lesions. Neurobiol Dis 74:14-24. doi:10.1016/j.nbd.2014.09.016
2. Bandura DR, Baranov VI, Ornatsky OI, Antonov A, Kinach R, Lou X, Pavlov S, Vorobiev S, Dick JE, Tanner SD (2009) Mass cytometry: technique for real time single cell multitarget immunoassay based on inductively coupled plasma time-of-flight mass spectrometry. Anal Chem 81:6813-6822. doi:10.1021/ac901049w
3. Barnett MH, Prineas JW (2004) Relapsing and remitting multiple sclerosis: pathology of the newly forming lesion. Ann Neurol 55:458-468. doi:10.1002/ana.20016
4. Bendall SC, Simonds EF, Qiu P, Amir el AD, Krutzik PO, Finck R, Bruggner RV, Melamed R, Trejo A, Ornatsky OI, Balderas RS, Plevritis SK, Sachs K, Pe'er D, Tanner SD, Nolan GP (2011) Single-cell mass cytometry of differential immune and drug responses across a human hematopoietic continuum. Science 332:687-696. doi:10.1126/science.1198704
5. Bennett ML, Bennett FC, Liddelow SA, Ajami B, Zamanian JL, Fernhoff NB, Mulinyawe SB, Bohlen CJ, Adil A, Tucker A, Weissman IL, Chang EF, Li G, Grant GA, Hayden Gephart MG, Barres BA (2016) New tools for studying microglia in the mouse and human CNS. Proc Natl Acad Sci U S A 113:E1738-1746. doi:10.1073/pnas.1525528113
6. Bodenmiller B, Zunder ER, Finck R, Chen TJ, Savig ES, Bruggner RV, Simonds EF, Bendall SC, Sachs K, Krutzik PO, Nolan GP (2012) Multiplexed mass cytometry profiling of cellular states perturbed by small-molecule regulators. Nat Biotechnol 30:858-867. doi:10.1038/nbt.2317
7. Bruck W, Porada P, Poser S, Rieckmann P, Hanefeld F, Kretzschmar HA, Lassmann H (1995) Monocyte/macrophage differentiation in early multiple sclerosis lesions. Ann Neurol 38:788-796. doi:10.1002/ana.410380514
8. Carpenter AE, Jones TR, Lamprecht MR, Clarke C, Kang IH, Friman O, Guertin DA, Chang JH, Lindquist RA, Moffat J, Golland P, Sabatini DM (2006) CellProfiler: image analysis software for identifying and quantifying cell phenotypes. Genome Biol 7:R100. doi:10.1186/gb-2006-7-10-r100
9. Carvajal-Hausdorf DE, Patsenker J, Stanton KP, Villarroel-Espindola F, Esch A, Montgomery RR, Psyrri A, Kalogeras KT, Kotoula V, Foutzilas G, Schalper KA, Kluger Y, Rimm DL (2019) Multiplexed (18-Plex) Measurement of Signaling Targets and Cytotoxic T Cells in Trastuzumab-Treated Patients using Imaging Mass Cytometry. Clin Cancer Res. doi:10.1158/1078-0432.CCR-18-2599
10. Chang Q, Ornatsky OI, Siddiqui I, Loboda A, Baranov VI, Hedley DW (2017) Imaging Mass Cytometry. Cytometry A 91:160-169. doi:10.1002/cyto.a.23053
11. Conde JR, Streit WJ (2006) Microglia in the aging brain. J Neuropathol Exp Neurol 65:199-203. doi:10.1097/01.jnen.0000202887.22082.63
12. Crabtree GR, Olson EN (2002) NFAT signaling: choreographing the social lives of cells. Cell 109 Suppl:S67-79
13. Ellingson BM, Zaw T, Cloughesy TF, Naeini KM, Lalezari S, Mong S, Lai A, Nghiemphu PL, Pope WB (2012) Comparison between intensity normalization techniques for dynamic susceptibility contrast (DSC)-MRI estimates of cerebral blood volume (CBV) in human gliomas. J Magn Reson Imaging 35:1472-1477. doi:10.1002/jmri.23600
14. Fischer MT, Sharma R, Lim JL, Haider L, Frischer JM, Drexhage J, Mahad D, Bradl M, van Horssen J, Lassmann H (2012) NADPH oxidase expression in active multiple

sclerosis lesions in relation to oxidative tissue damage and mitochondrial injury. Brain 135:886-899. doi:10.1093/brain/aws012

15. Frischer JM, Bramow S, Dal-Bianco A, Lucchinetti CF, Rauschka H, Schmidbauer M, Laursen H, Sorensen PS, Lassmann H (2009) The relation between inflammation and neurodegeneration in multiple sclerosis brains. Brain 132:1175-1189. doi:10.1093/brain/awp070
16. Frischer JM, Weigand SD, Guo Y, Kale N, Parisi JE, Pirko I, Mandrekar J, Bramow S, Metz I, Bruck W, Lassmann H, Lucchinetti CF (2015) Clinical and pathological insights into the dynamic nature of the white matter multiple sclerosis plaque. Ann Neurol 78:710-721. doi:10.1002/ana.24497
17. Gay FW, Drye TJ, Dick GW, Esiri MM (1997) The application of multifactorial cluster analysis in the staging of plaques in early multiple sclerosis. Identification and characterization of the primary demyelinating lesion. Brain 120 (Pt 8):1461-1483
18. Haider L, Simeonidou C, Steinberger G, Hametner S, Grigoriadis N, Deretzi G, Kovacs GG, Kutzelnigg A, Lassmann H, Frischer JM (2014) Multiple sclerosis deep grey matter: the relation between demyelination, neurodegeneration, inflammation and iron. J Neurol Neurosurg Psychiatry 85:1386-1395. doi:10.1136/jnnp-2014-307712
19. Han G, Spitzer MH, Bendall SC, Fantl WJ, Nolan GP (2018) Metal-isotope-tagged monoclonal antibodies for high-dimensional mass cytometry. Nat Protoc 13:2121-2148. doi:10.1038/s41596-018-0016-7
20. Hauser SL, Bar-Or A, Comi G, Giovannoni G, Hartung HP, Hemmer B, Lublin F, Montalban X, Rammohan KW, Selmaj K, Traboulsee A, Wolinsky JS, Arnold DL, Klingelschmitt G, Masterman D, Fontoura P, Belachew S, Chin P, Mairon N, Garren H, Kappos L, Opera I, Investigators OIC (2017) Ocrelizumab versus Interferon Beta-1a in Relapsing Multiple Sclerosis. N Engl J Med 376:221-234. doi:10.1056/NEJMoa1601277
21. Hauser SL, Waubant E, Arnold DL, Vollmer T, Antel J, Fox RJ, Bar-Or A, Panzara M, Sarkar N, Agarwal S, Langer-Gould A, Smith CH, Group HT (2008) B-cell depletion with rituximab in relapsing-remitting multiple sclerosis. N Engl J Med 358:676-688. doi:10.1056/NEJMoa0706383
22. Jones TR, Kang IH, Wheeler DB, Lindquist RA, Papallo A, Sabatini DM, Golland P, Carpenter AE (2008) CellProfiler Analyst: data exploration and analysis software for complex image-based screens. BMC Bioinformatics 9:482. doi:10.1186/1471-2105-9-482
23. Kebir H, Kreymborg K, Ifergan I, Dodelet-Devillers A, Cayrol R, Bernard M, Giuliani F, Arbour N, Becher B, Prat A (2007) Human TH17 lymphocytes promote blood-brain barrier disruption and central nervous system inflammation. Nat Med 13:1173-1175. doi:10.1038/nm1651
24. Koulieris E, Panayiotidis P, Harding SJ, Kafasi N, Maltezas D, Bartzis V, Tzenou T, Dimou M, Georgiou G, Mirbahai L, Bradwell AR, Kyrtsonis MC (2012) Ratio of involved/uninvolved immunoglobulin quantification by Hevylite assay: clinical and prognostic impact in multiple myeloma. Exp Hematol Oncol 1:9. doi:10.1186/2162-3619-1-9
25. Kuhlmann T, Ludwin S, Prat A, Antel J, Bruck W, Lassmann H (2017) An updated histological classification system for multiple sclerosis lesions. Acta Neuropathol 133:13-24. doi:10.1007/s00401-016-1653-y
26. Larochelle C, Metz I, Lecuyer MA, Terouz S, Roger M, Arbour N, Bruck W, Prat A (2017) Immunological and pathological characterization of fatal rebound MS activity following natalizumab withdrawal. Mult Scler 23:72-81. doi:10.1177/1352458516641775

27. Li H, Cuzner ML, Newcombe J (1996) Microglia-derived macrophages in early multiple sclerosis plaques. Neuropathol Appl Neurobiol 22:207-215
28. Lucchinetti C, Bruck W, Parisi J, Scheithauer B, Rodriguez M, Lassmann H (2000) Heterogeneity of multiple sclerosis lesions: implications for the pathogenesis of demyelination. Ann Neurol 47:707-717
29. Luchetti S, Fransen NL, van Eden CG, Ramaglia V, Mason M, Huitinga I (2018) Progressive multiple sclerosis patients show substantial lesion activity that correlates with clinical disease severity and sex: a retrospective autopsy cohort analysis. Acta Neuropathol 135:511-528. doi:10.1007/s00401-018-1818-y
30. Ma B, Yu J, Xie C, Sun L, Lin S, Ding J, Luo J, Cai H (2015) Toll-Like Receptors Promote Mitochondrial Translocation of Nuclear Transcription Factor Nuclear Factor of Activated T-Cells in Prolonged Microglial Activation. J Neurosci 35:10799-10814. doi:10.1523/JNEUROSCI.2455-14.2015
31. Machado-Santos J, Saji E, Troscher AR, Paunovic M, Liblau R, Gabriely G, Bien CG, Bauer J, Lassmann H (2018) The compartmentalized inflammatory response in the multiple sclerosis brain is composed of tissue-resident CD8+ T lymphocytes and B cells. Brain 141:2066-2082. doi:10.1093/brain/awy151
32. Marik C, Felts PA, Bauer J, Lassmann H, Smith KJ (2007) Lesion genesis in a subset of patients with multiple sclerosis: a role for innate immunity? Brain 130:2800-2815. doi:10.1093/brain/awm236
33. Perry VH, Nicoll JA, Holmes C (2010) Microglia in neurodegenerative disease. Nat Rev Neurol 6:193-201. doi:10.1038/nrneurol.2010.17
34. Podjaski C, Alvarez JI, Bourbonniere L, Larouche S, Terouz S, Bin JM, Lecuyer MA, Saint-Laurent O, Larochelle C, Darlington PJ, Arbour N, Antel JP, Kennedy TE, Prat A (2015) Netrin 1 regulates blood-brain barrier function and neuroinflammation. Brain 138:1598-1612. doi:10.1093/brain/awv092
35. Popescu BF, Frischer JM, Webb SM, Tham M, Adiele RC, Robinson CA, Fitz-Gibbon PD, Weigand SD, Metz I, Nehzati S, George GN, Pickering IJ, Bruck W, Hametner S, Lassmann H, Parisi JE, Yong G, Lucchinetti CF (2017) Pathogenic implications of distinct patterns of iron and zinc in chronic MS lesions. Acta Neuropathol 134:45-64. doi:10.1007/s00401-017-1696-8
36. Robinson AP, Harp CT, Noronha A, Miller SD (2014) The experimental autoimmune encephalomyelitis (EAE) model of MS: utility for understanding disease pathophysiology and treatment. Handb Clin Neurol 122:173-189. doi:10.1016/B978-0-444-52001-2.00008-X
37. Rojas OL, Probstel AK, Porfilio EA, Wang AA, Charabati M, Sun T, Lee DSW, Galicia G, Ramaglia V, Ward LA, Leung LYT, Najafi G, Khaleghi K, Garcillan B, Li A, Besla R, Naouar I, Cao EY, Chiaranunt P, Burrows K, Robinson HG, Allanach JR, Yam J, Luck H, Campbell DJ, Allman D, Brooks DG, Tomura M, Baumann R, Zamvil SS, Bar-Or A, Horwitz MS, Winer DA, Mortha A, Mackay F, Prat A, Osborne LC, Robbins C, Baranzini SE, Gommerman JL (2019) Recirculating Intestinal IgA-Producing Cells Regulate Neuroinflammation via IL-10. Cell 176:610-624 e618. doi:10.1016/j.cell.2018.11.035
38. Satoh J, Kino Y, Asahina N, Takitani M, Miyoshi J, Ishida T, Saito Y (2016) TMEM119 marks a subset of microglia in the human brain. Neuropathology 36:39-49. doi:10.1111/neup.12235
39. Serafini B, Zandee S, Rosicarelli B, Scorsi E, Veroni C, Larochelle C, D'Alfonso S, Prat A, Aloisi F (2018) Epstein-Barr virus-associated immune reconstitution inflammatory syndrome as possible cause of fulminant multiple sclerosis relapse after natalizumab interruption. J Neuroimmunol 319:9-12. doi:10.1016/j.jneuroim.2018.03.011

911 40. Storch MK, Piddlesden S, Haltia M, Iivanainen M, Morgan P, Lassmann H (1998) Multiple
912 sclerosis: in situ evidence for antibody- and complement-mediated demyelination. Ann
913 Neurol 43:465-471. doi:10.1002/ana.410430409
914 41. Sun D, Whitaker JN, Huang Z, Liu D, Coleclough C, Wekerle H, Raine CS (2001) Myelin
915 antigen-specific CD8+ T cells are encephalitogenic and produce severe disease in
916 C57BL/6 mice. J Immunol 166:7579-7587
917 42. Vogel DY, Vereyken EJ, Glim JE, Heijnen PD, Moeton M, van der Valk P, Amor S,
918 Teunissen CE, van Horssen J, Dijkstra CD (2013) Macrophages in inflammatory
919 multiple sclerosis lesions have an intermediate activation status. J Neuroinflammation
920 10:35. doi:10.1186/1742-2094-10-35
921 43. Wang Z, Zhu L, Nguyen THO, Wan Y, Sant S, Quinones-Parra SM, Crawford JC, Eltahla
922 AA, Rizzetto S, Bull RA, Qiu C, Koutsakos M, Clemens EB, Loh L, Chen T, Liu L,
923 Cao P, Ren Y, Kedzierski L, Kotsimbos T, McCaw JM, La Gruta NL, Turner SJ, Cheng
924 AC, Luciani F, Zhang X, Doherty PC, Thomas PG, Xu J, Kedzierska K (2018) Clonally
925 diverse CD38(+)HLA-DR(+)CD8(+) T cells persist during fatal H7N9 disease. Nat
926 Commun 9:824. doi:10.1038/s41467-018-03243-7
927 44. Zrzavy T, Hametner S, Wimmer I, Butovsky O, Weiner HL, Lassmann H (2017) Loss of
928 'homeostatic' microglia and patterns of their activation in active multiple sclerosis.
929 Brain 140:1900-1913. doi:10.1093/brain/awx113

930 **Figure 1**

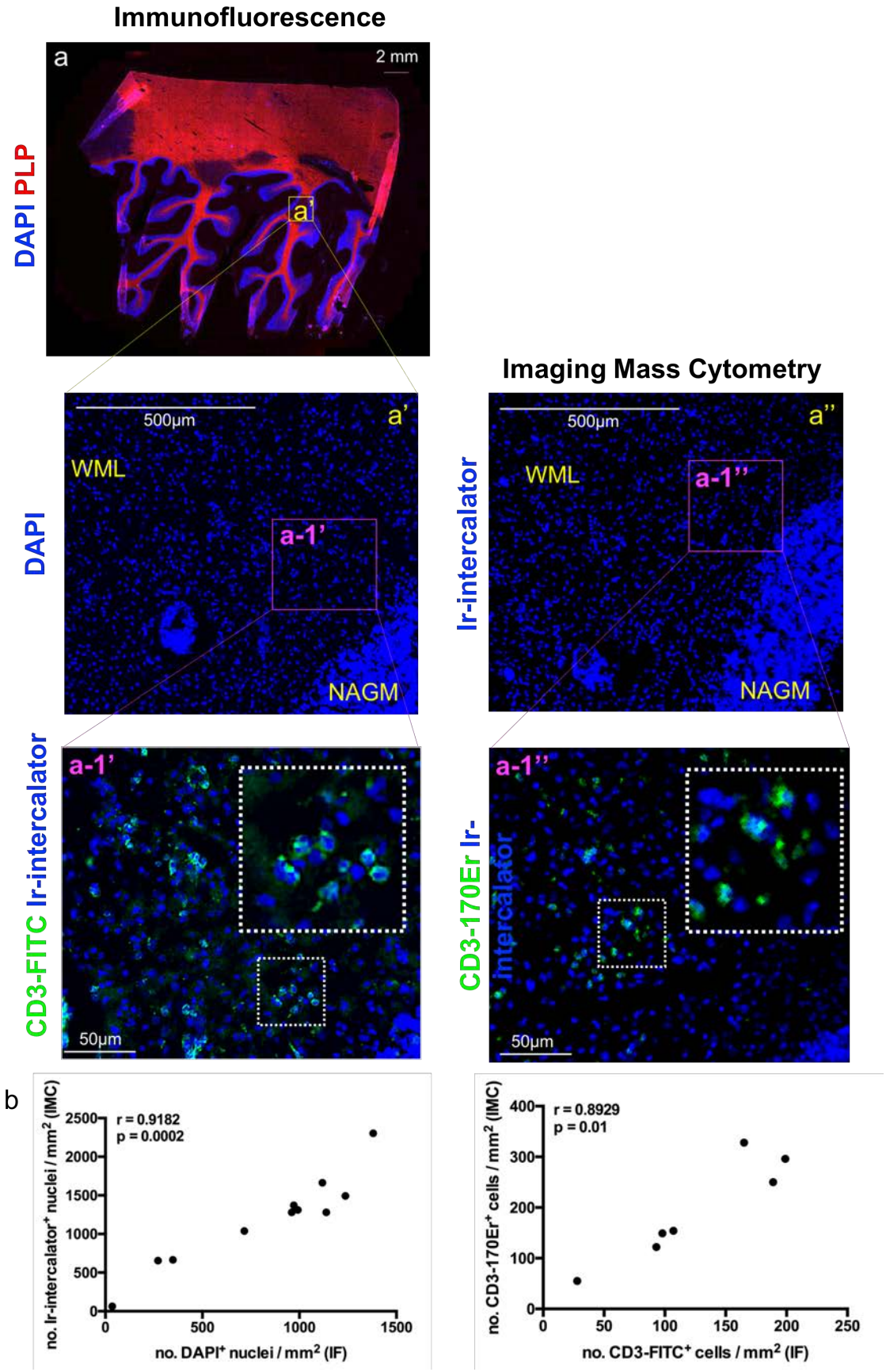

931 **Figure 2**

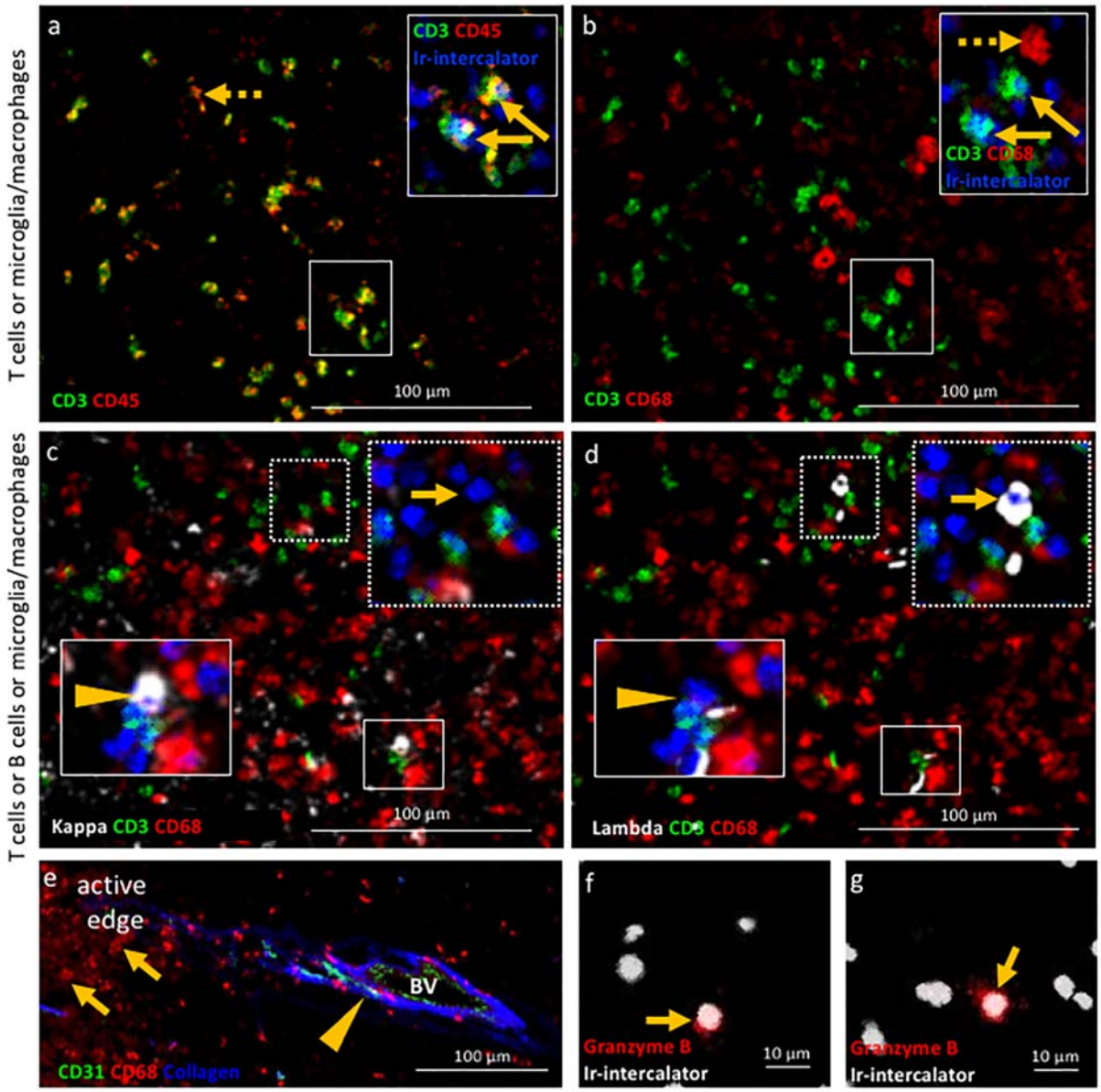

932 **Figure 3**

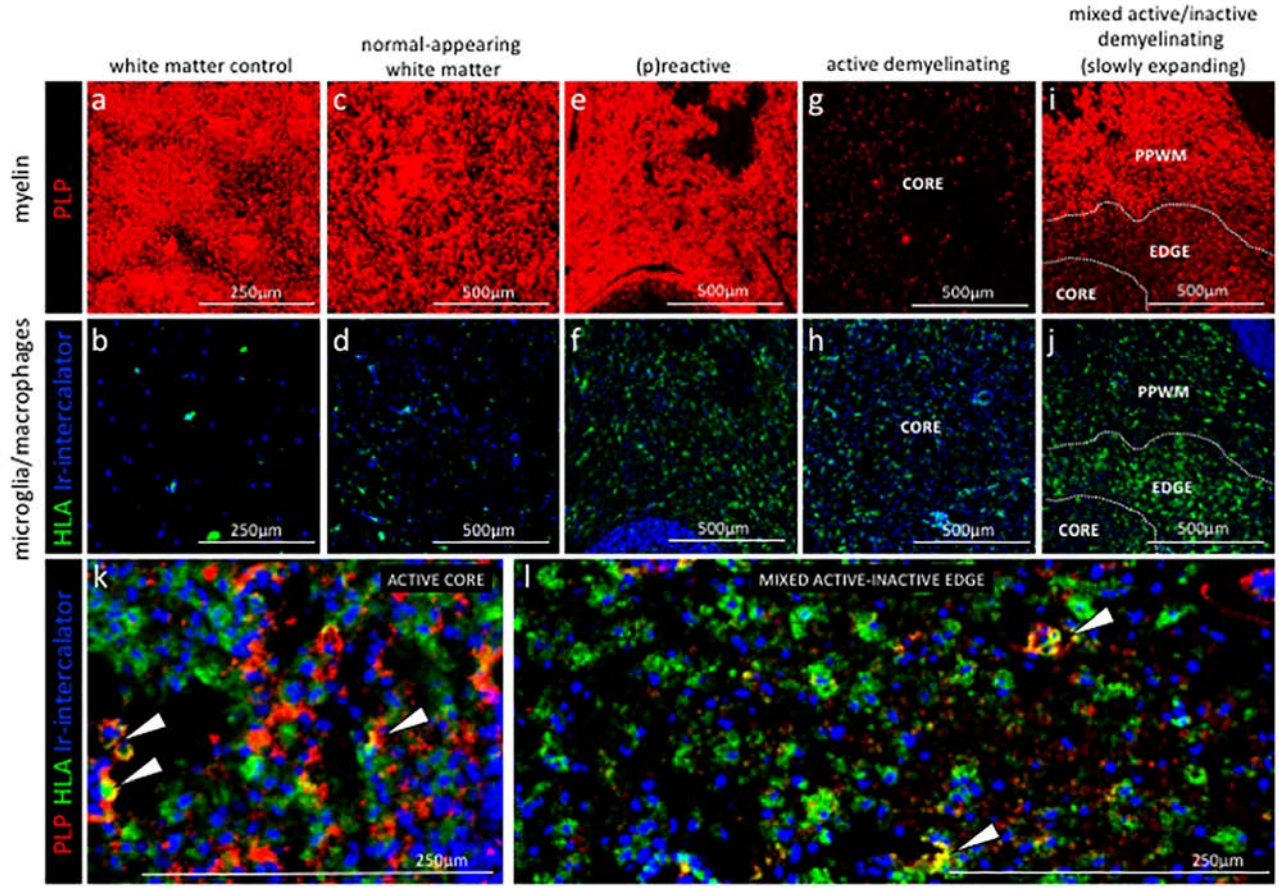

933 **Figure 4**

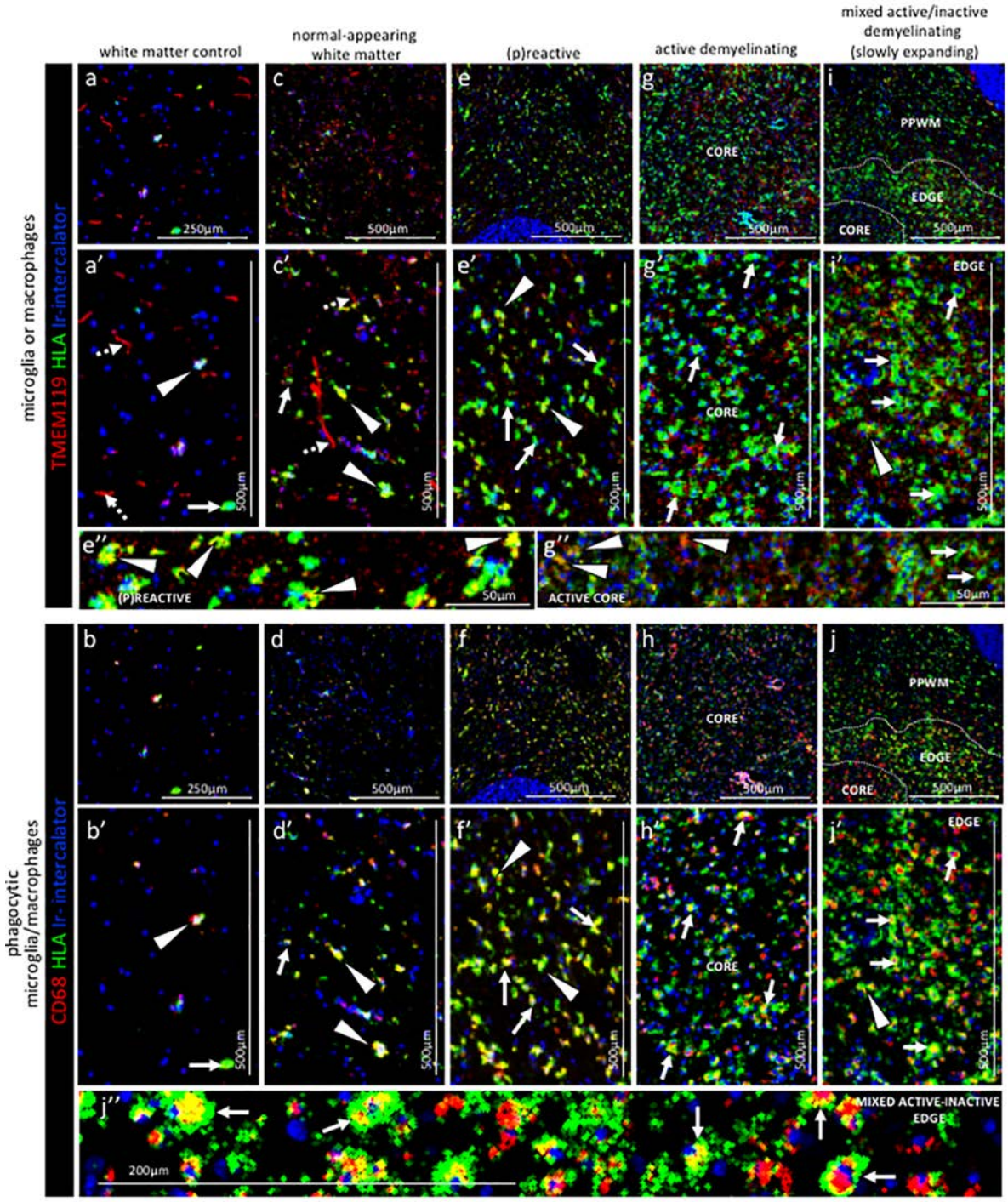

934 **Figure 5**

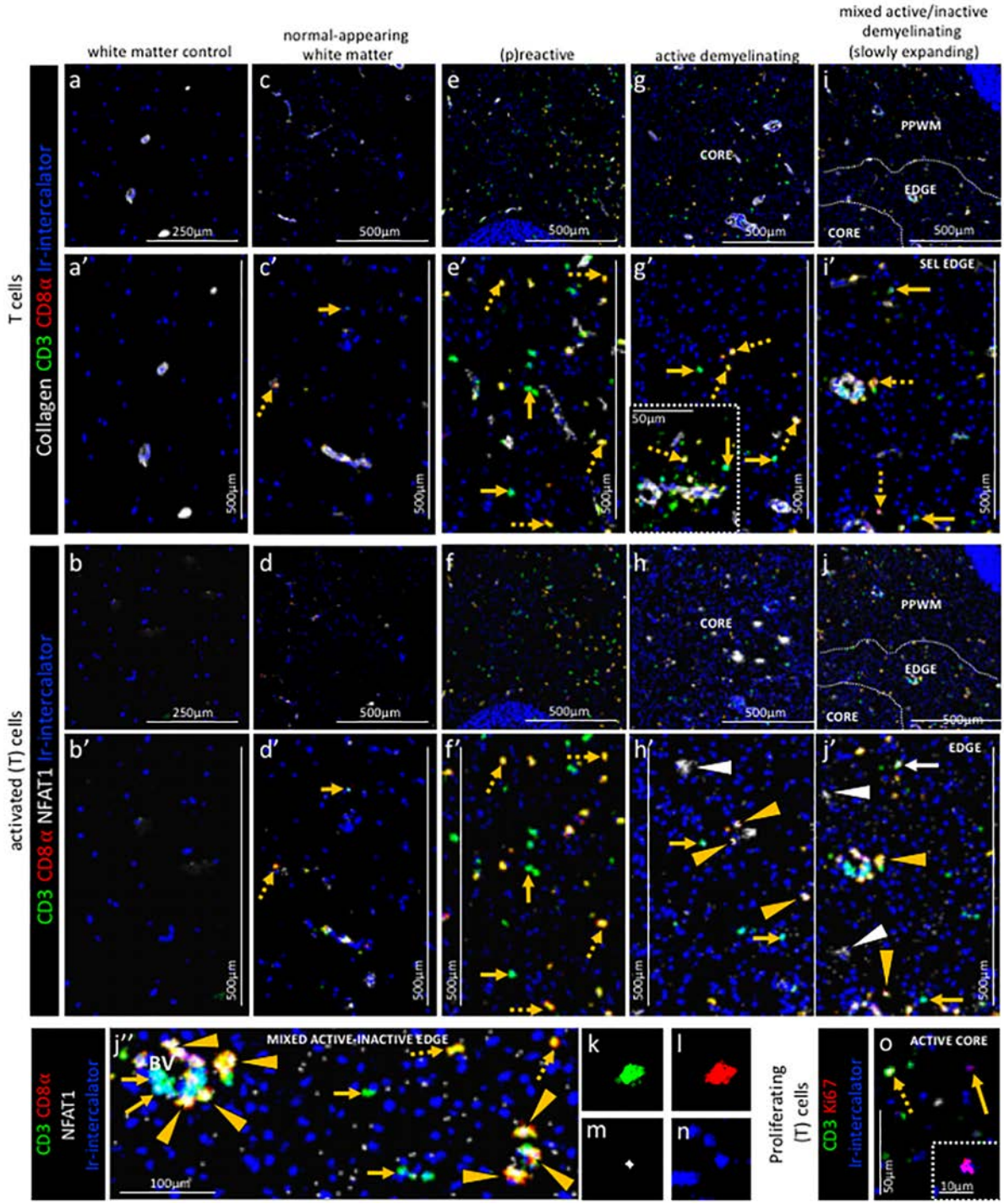

935 **Figure 6**

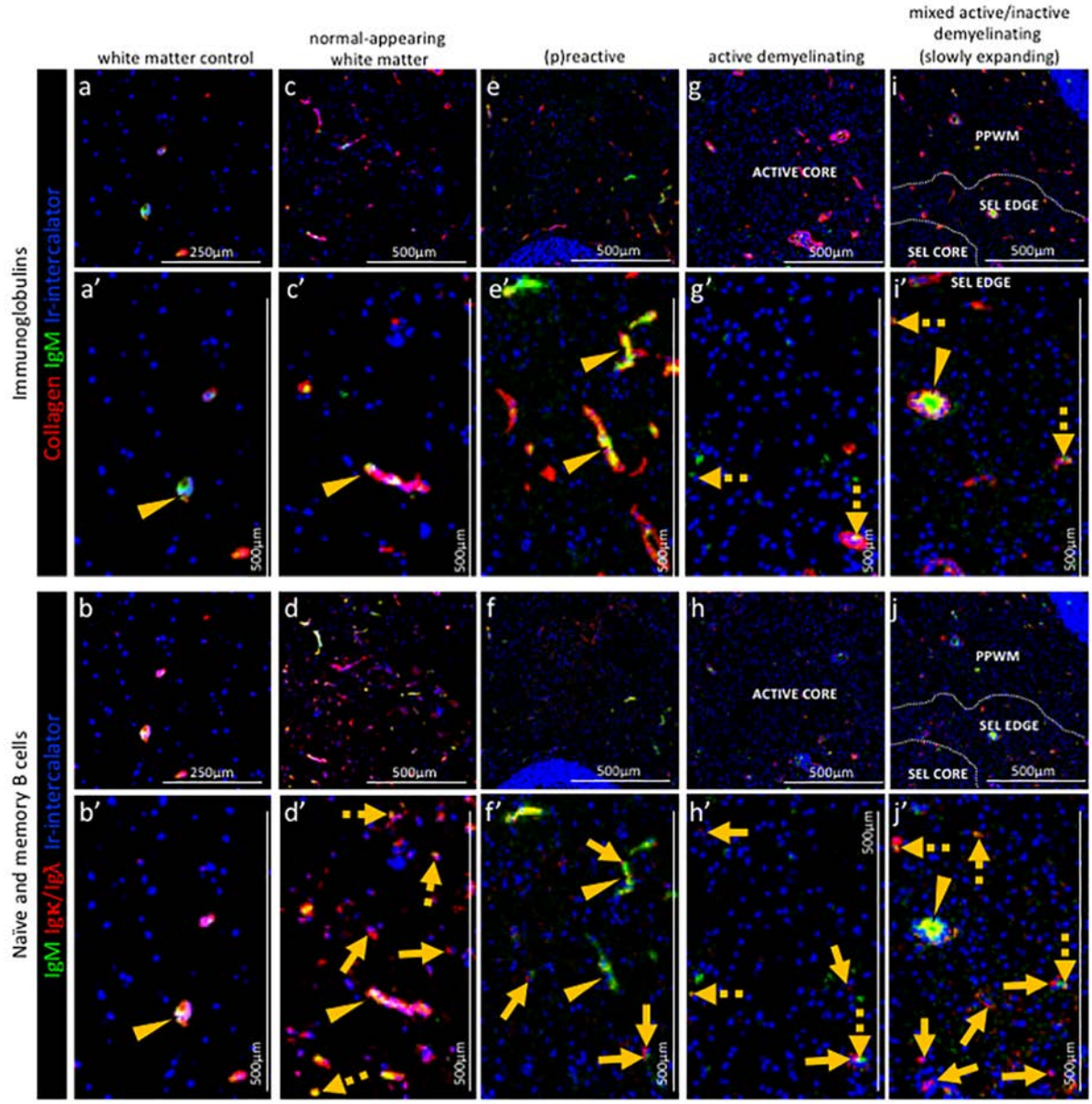

936 **Figure 7**

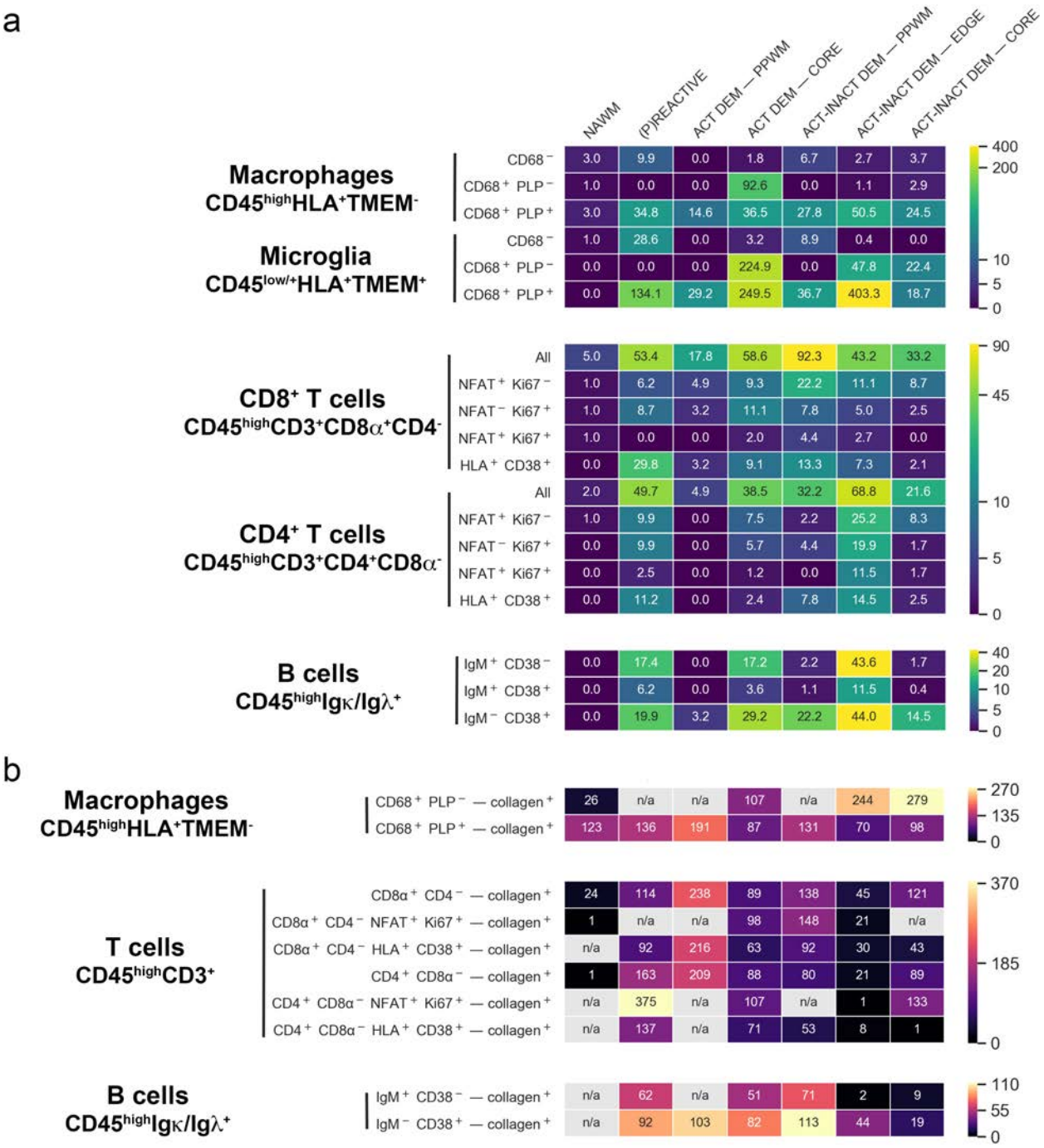

937

Table 1. Lesion types and regions of interest

Case	**Tissue Block** **(anatomical location)**	**Lesion Type**	**Region of interest**
C, 95-056	A (superior frontal gyrus)		WMC
MS, AB129	CL3a (cerebellum)		NAWM
		2x Active demyelinating (pattern II)	PPWM, center
		3x Mixed active/inactive demyelinating	PPWM, edge, core
	CR4a (cerebellum)		NAWM
		(p)reactive	
		3x Active demyelinating (pattern II)	center
		2x Mixed active/inactive demyelinating	edge, core

C, control; MS, multiple sclerosis; WMC, white matter of control; NAWM, normal-appearing white matter; PPWM, periplaque white matter.

938

939

Table 2. Antibodies used for Imaging Mass Cytometry

Antibody	Target	Metal Tag	Antibody Clone	Concentration (μg/ml)	Source (Catalogue)
Ir-Intercalator	DNA	Ir191 Ir193		0.5	Fluidigm (201192A)
PLP (proteolipid protein)	Myelin	141Pr	Plpc1	20, 40[a], 10[b]	Bio-Rad (MCA839G)
CD38	Leukocytes	167Er	HIT2	0.5	Fluidigm (3167001B)
CD45	Leukocytes/ Macrophages	154Sm	HI30	0.5	Fluidigm (3154001B)
CD68	Lysosomal Marker (phagocytic cells)	159Tb	KP1	10	Fluidigm (3159035D)
HLA (human leukocyte antigen)	Microglia/ Macrophages	147Sm	LN3	5,10[a], 5[b]	Abcam (Ab55152)
TMEM119	Microglia	155Gd	Polyclonal	10, 5[a]	Sigma-Aldrich (HPA051870)
CD3	T Cells	170Er	UCHT1	10	Fluidigm (3170001B)
CD4	$CD4^+$ T Cells	176Yb	SK3	5, 25[a]	BioLegend (344602)
CD8α	$CD8^+$T cells	162Dy	RPA-T8	10	Fluidigm (3162015B)
Granzyme B	CD8+ T Cell Activation	171Yb	GB11	20, 50[a]	ThermoFisher Scientific (MA1-80734)
Ig Kappa	Immunoglobulin (light chain)	160Gd	MHK-49	0.33	Fluidigm (3160006B)
Ig Lambda	Immunoglobulin (light chain)	151Eu	MHL-38	0.33	Fluidigm (3151004B)
IgM	Immunoglobulin	172Yb	MHM-88	2	Fluidigm (3172004B)
Collagen	Blood Vessels	169Tm	Polyclonal	0.25	Fluidigm (3169023D)
CD31	Endothelial cells	145Nd	C31.3+ C31.7+ C31.10	10	LSBio (LS-C390863)
NFAT1 (Nuclear Factor of activated T cells)	Cell activation	143Nd	D43B1	20	Fluidigm (3143023A)
Ki67	Cell Proliferation	168Er	Ki-67	10	Fluidigm (3168001B)

[a],[b]concentration of the unlabeled antibody by immunofluorescence[a] or immunohistochemistry[b]

940

Table 3. Antibody panels for the identification of functional cell types by IMC

Functional Cell Type	**Antibody Panel**
Macrophages and microglia	
Macrophages	$CD45^{high}HLA^{+}TMEM119^{-}$
Activated macrophages	$CD45^{high}HLA^{+}TMEM119^{-}CD68^{+}PLP^{-}$
Demyelinating macrophages	$CD45^{high}HLA^{+}TMEM119^{-}CD68^{+}PLP^{+}$
Microglia	$CD45^{low/+}HLA^{+}TMEM119^{+}$
Activated microglia	$CD45^{low/+}HLA^{+}TMEM119^{+}CD68^{+}PLP^{-}$
Demyelinating microglia	$CD45^{low/+}HLA^{+}TMEM119^{+}CD68^{+}PLP^{+}$
T Cells	
$CD8^{+}$ T cells	$CD45^{+}CD3^{+}CD8\alpha^{+}CD4^{-}$
Proliferating $CD8^{+}$ T cells	$CD45^{+}CD8\alpha^{+}CD3^{+}CD4^{-}Ki67^{+}$
Activated $CD8^{+}$ T cells	$CD45^{+}CD3^{+}CD8\alpha^{+}CD4^{-}NFAT^{+}$
Activated and proliferating $CD8^{+}$ T cells	$CD45^{+}CD3^{+}CD8\alpha^{+}CD4^{-}NFAT^{+}Ki67^{+}$
"Chronically activated" $CD8^{+}$ T cells	$CD45^{+}CD3^{+}CD8\alpha^{-}CD8^{+}CD38^{+}HLA^{+}$
$CD4^{+}$ T cells	$CD45^{+}CD3^{+}CD8\alpha^{-}CD4^{+}$
Proliferating $CD4^{+}$ T cells	$CD45^{+}CD8\alpha^{-}CD3^{+}CD4^{+}Ki67^{+}$
Activated $CD4^{+}$ T cells	$CD45^{+}CD3^{+}CD8\alpha^{-}CD4^{+}NFAT^{+}$
Activated and proliferating $CD4^{+}$ T cells	$CD45^{+}CD3^{+}CD8\alpha^{-}CD4^{+}NFAT^{+}Ki67^{+}$
"Chronically activated" $CD4^{+}$ T cells	$CD45^{+}CD3^{+}CD8\alpha^{-}CD4^{+}CD38^{+}HLA^{+}$
B Cells	
Naïve B Cells	$CD45^{+}Ig\kappa/Ig\lambda^{+}IgM^{+}CD38^{-}$
IgM memory B cells	$CD45^{+}Ig\kappa/Ig\lambda^{+}IgM^{+}CD38^{+}$
Switched memory B cells	$CD45^{+}Ig\kappa/Ig\lambda^{+}IgM^{-}CD38^{+}$

941

Figure 1 Comparing IMC to IF in MS lesions. Two serial sections were assessed: one used for immunofluorescence (IF, **a and a'**) and one dedicated to Imaging Mass Cytometry (IMC, **a''**). The region of interest (**a'**) was guided by the immunofluorescence staining with anti-PLP (proteolipid protein, shown in red to visualize myelin), and DAPI (shown in blue to visualize nuclei) (**a**) for the identification of lesion location and type (see **Figure 1 – Figure Supplement 1**). The entire region of interest on a serial section was subjected to IMC, according to the work flow shown in **Figure 1 – Figure Supplement 2**. Staining with Iridium (Ir)-intercalator is shown in blue to visualize DNA in nuclei. A blow up area (referred to as **a-1'** for IF and **a-1''** for IMC) of the region of interest within an active lesion, was also stained with fluorochrome conjugated anti-CD3 (a-1') or metal conjugated anti-CD3 (a-1"), both depicted in green. WML, white matter lesion; NAGM, normal-appearing grey matter. (**b**) Spearman correlation coefficient, showing a significant positive correlation between the number of nuclei identified with DAPI by IF and the number of nuclei identified with Ir-intercalator by IMC (n=11, coefficient, r=0.9182, p=0.0002). (**c**) Spearman correlation coefficient, showing a significant positive correlation between the number of $CD3^+$ T cells identified with fluorochrome-conjugated antibody by IF and the number of $CD3^+$ T cells identified with metal-conjugated antibody by IMC (n=7, coefficient, r=0.8929, p=0.01).

Figure 2 Validation of IMC specificity in MS lesions. (**a**) Overlay of CD3 (green) and CD45 (red) identifies $CD3^+CD45^+$ T cells (solid arrows) and $CD3^-CD45^+$ leukocytes other than T cells (dotted arrow). (**b**) Overlay of CD3 (green) and CD68 (red) identifies $CD3^+CD68^-$ T cells (solid arrows) and $CD3^-CD68^+$ microglia /macrophages (dotted arrow). Note that the solid arrows in a and b indicates the same $CD3^+CD45^+CD68^-$ T cells. (**c**) Overlay of κ (white), CD3 (green) and CD68 (red) and (**d**) overlay of λ (white), CD3 (green) and CD68 (red) identify

967 κ^+CD3$^-$CD68$^-$ B cells (arrow head in **c**) that are λ^-CD3$^-$CD68$^-$ (arrow head in **d**) and κ^-CD3$^-$
968 CD68$^-$ B cells (arrow in **c**) that are λ^+CD3$^-$CD68$^-$ (arrow in **d**), as expected based on the allelic
969 exclusion of κ and λ. (**e**) Overlay of CD31 (green), CD68 (red) and Collagen (blue) identifies
970 CD31$^+$Collagen$^+$CD68$^-$ endothelial cells (arrow head) and CD31$^-$Collagen$^-$
971 CD68$^+$ microglia/macrophages (arrows). (**f, g**) Granzyme B$^+$ cells (arrows). Images in **a** and
972 **b** as well as images in **c** and **d** are from the same areas of an active demyelinating lesion. Image
973 in **e** are from the edge of an active demyelinating lesion. Images in **f** and **g** are from the center
974 of an active demyelinating lesion.
975
976 **Figure 3 Staging of MS lesions by IMC.** Representative mass cytometry images of white
977 matter areas of healthy control (**a, f**), MS normal-appearing white matter (block no. CR4A)
978 (**b, g**), MS (p)reactive lesion (block no. CR4A) (**c, h**), MS active demyelinating lesion (block
979 no. CR4A) (**d-i**) and an MS slowly expanding lesion (block no. CL3A) (**e-j**). For each region
980 of interest, we show the same area simultaneously labeled with markers of myelin
981 (proteolipid protein, PLP), antigen presentation (human leukocyte antigen, HLA) to detect
982 microglia/macrophages and DNA (intercalator). Images of PLP (red) (**a-e**) and overlay of
983 HLA (green) and intercalator (blue) (**f-i**) show the lesion activity in staged MS lesions
984 compared to control white matter and normal-appearing white matter. (**k, l**) Overlay of PLP,
985 HLA and intercalator show microglia/macrophages containing PLP$^+$ myelin protein in the
986 core of an active lesion (**k**) and in the edge of a slowly expanding lesion (**l**), indicative of
987 demyelinating activity. PPWM, periplaque white matter; BV, blood vessel.
988
989 **Figure 4 Pattern of microglia or macrophage activity in different stages of MS lesions by**
990 **IMC.** Representative mass cytometry images of control white matter (**a, a', b, b'**), normal-
991 appearing white matter (block no. CR4A) (**c, c', d, d'**), (p)reactive lesion (block no. CR4A) (**e,**

992 **e', f, f'**), active demyelinating lesion (block no. CR4A) (**g, g', h, h'**) and slowly expanding
993 lesion (block no. CL3A) (**i, i', j, j'**). For each region of interest, we show the same area
994 simultaneously labeled with markers of antigen presentation (human leukocyte antigen, HLA)
995 to detect microglia and/or macrophages, TMEM119 to detect microglia, lysosomes (CD68) to
996 detect phagocytic cells and DNA (Ir-intercalator). (**a, a'- i, i'**) Overlay of TMEM119 (red),
997 HLA (green) and Ir-intercalator (blue) identifies $TMEM119^{+}HLA^{-}$ resting microglia with thin
998 elongated processes (dotted arrows in **a' and c'**) and $TMEM119^{+}HLA^{+}$ activated microglia
999 (arrows head in **a',c', e', i' and e''**) or $TMEM119^{-}HLA^{+}$ activated macrophages (solid arrows
1000 in **a', c', e', g', i' and g''**). (**b, b'-j, j''**) Overlay of CD68 (red), HLA (green) and intercalator
1001 (blue) identifies $HLA^{+}CD68^{+}$ phagocytic microglia/macrophages. PPWM, periplaque white
1002 matter; BV, blood vessel.

1003 **Figure 5 Pattern of T cell subpopulations in different stages of MS lesions by IMC.**
1004 Representative mass cytometry images of white matter of control (**a, a', b, b'**), normal-
1005 appearing white matter (block no. CR4A) (**c, c', d, d'**), (p)reactive lesion (block no. CR4A) (**e,**
1006 **e', f, f'**), active demyelinating lesion (block no. CR4A) (**g, g', h, h', o**) and slowly expanding
1007 lesion (block no. CL3A) (**i, i', j-n**). For each region of interest, we show the same area
1008 simultaneously labeled with anti-collagen antibodies to visuzliae blood vessels, all T cells
1009 (CD3), CD8α T cells, cell proliferation (Ki67) and DNA (Ir-intercalator). (**a, a'- i, i'**) Overlay
1010 of collagen (white), CD3 (green), CD8α (red) and Ir-intercalator (blue) identifies $CD3^{+}CD8\alpha^{+}$
1011 T cells (dotted arrows in **c', e', g' and i'**), $CD3^{+}CD8\alpha^{-}$ (therefore by exclusion putative $CD4^{+}$)
1012 T cells (solid arrows in **c', e', g' and i'**) and $collagen^{+}$ blood vessels. (**b-b'-j, j''**) Overlay of
1013 CD3 (in green), CD8α (red), NFAT1 (in white) and Ir-intercalator (in blue) identifies
1014 $CD3^{+}CD8\alpha^{+}NFAT1^{+}$ T cells (yellow arrow head in **h', j' and j''**) and $CD3^{+}CD8\alpha^{-}NFAT1^{+}$
1015 (putative $CD4^{+}$) T cells (white solid arrow in **j'**). $CD3^{-}CD8\alpha^{-}NFAT1^{+}$ cells are also detected

(white arrow head in **h' and j'**). (**o**) Overlay of CD3 (in green), Ki67 (red) and Ir-intercalator (in blue) identifies $CD3^{+}Ki67^{+}$ proliferating Tcells (dotted arrow) and $CD3^{-}Ki67^{+}$ proliferating cells other than T cells (solid arrows and inset). PPWM, periplaque white matter.

Figure 6 Pattern of immunoglobulins and B cell subpopulations in different stages of MS lesions by IMC. Representative mass cytometry images of white matter of control (**a, a', b, b'**), normal-appearing white matter (block no. CR4A) (**c, c', d, d'**), a (p)reactive lesion (block no. CR4A) (**e, e', f, f'**), an active demyelinating lesion (block no. CR4A) (**g, g', h, h', o**) and a slowly expanding lesion (block no. CL3A) (**i, i', j-n**). For each region of interest, we show the same area simultaneously labeled with markers of endothelial cells (collagen) to detect blood vessels, immunoglobulin M (IgM), the κ or λ light chain of immunoglobulins (Igκ/Igλ) to detect B cells and DNA (Ir-intercalator). (**a, a-i, i'**) Overlay of collagen (red), IgM (green) and Ir-intercalator (blue) identifies cellular (intercalator-associated, dotted arrows in g' and i') and non-cellular (free immunoglobulin, arrows head in **a', c', e', i'**) IgM in the parenchyma or within $collagen^{+}$ blood vessels. (**b, b'-j, j'**) Overlay of IgM (green), Igκ/Igλ (red) and Ir-intercalator (blue) identifies $Igκ/Igλ^{+}IgM^{+}$ naïve and IgM memory B cells (dotted arrow in **d', h' and j'**) and $Igκ/Igλ^{+}IgM^{-}$ class switch B cells (solid arrows in **d', f', h' and j'**).

Figure 7 Density of immune cell subsets in different stages of MS lesions and their distance from blood vessels by IMC. (**a**) Cell counts are provided as number of cells per mm^2 of region of interest. The category of cells is defined according to the expression of cell-specific and functional markers as indicated and also described in **Table 3**. (**b**) Distance between defined categories of cells and blood vessels ($collagen^{+}$) are provided in μm. NAWM, normal-appearing white matter; PPWM, periplaque white matter; Act dem, active demyelinating; act inact dem, active-inactive demyelinating. The single-cell segmentation strategy is shown in

1041 **Figure 7 – Figure Supplement 1**. The Positive and negative "gates" used to identify each cell
1042 subset were established based on the quadrants laid out in **Figure 7 – Figure Supplement 2**.
1043 Please see the section "Gating strategy for quantitative analysis of T cell, B cell, macrophage
1044 and microglial cell subsets" in the materials and methods. The gating strategy used for the
1045 generation of heat maps is laid out in **Figure 7 – Figure Supplement 3**. Source files used for
1046 the quantitative analysis are provided in **Figure 7 – Source data 1**.
1047

1048 **Figure Supplements**

Figure 1 – Figure Supplement 1

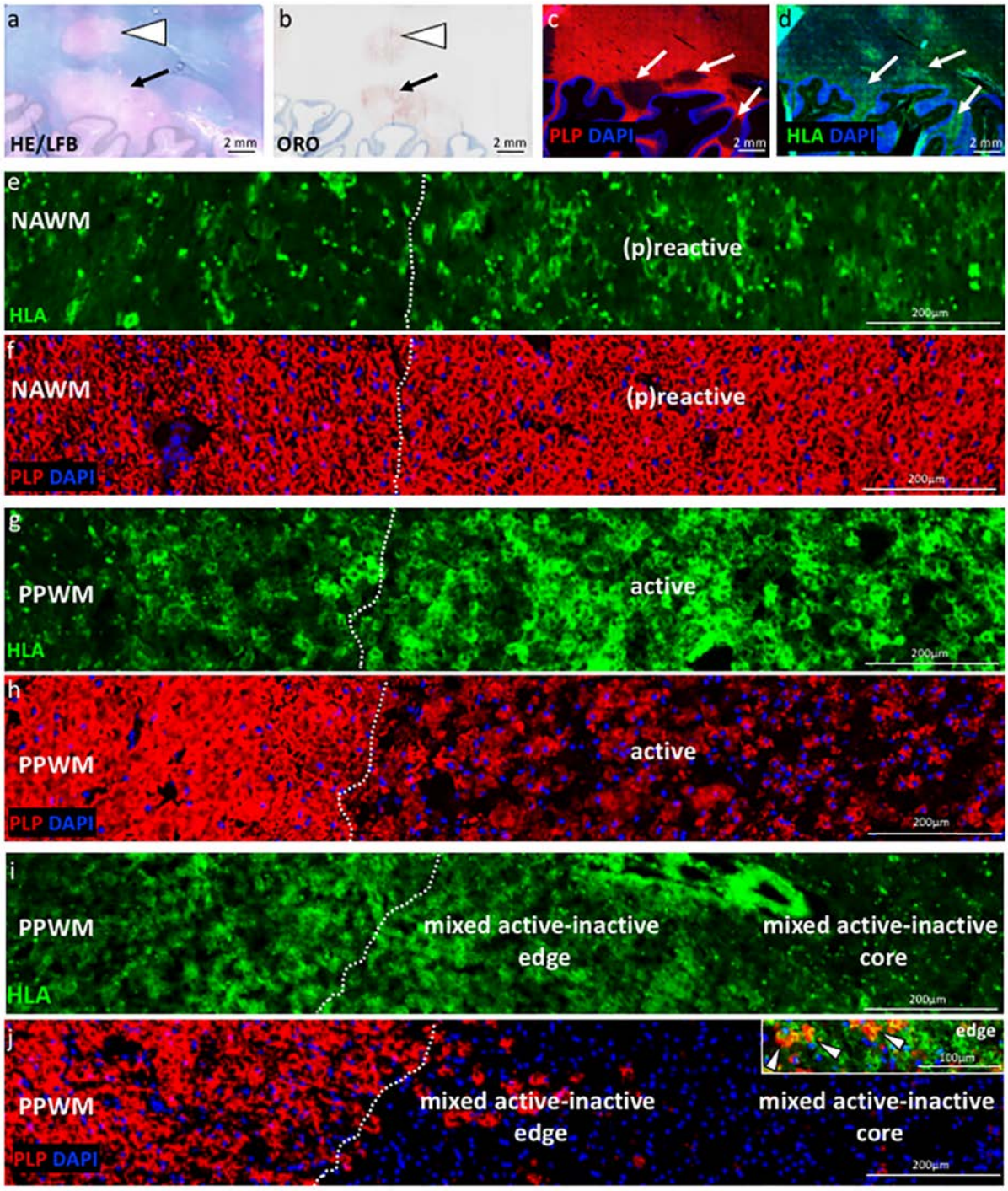

Figure 1 – Figure Supplement 2

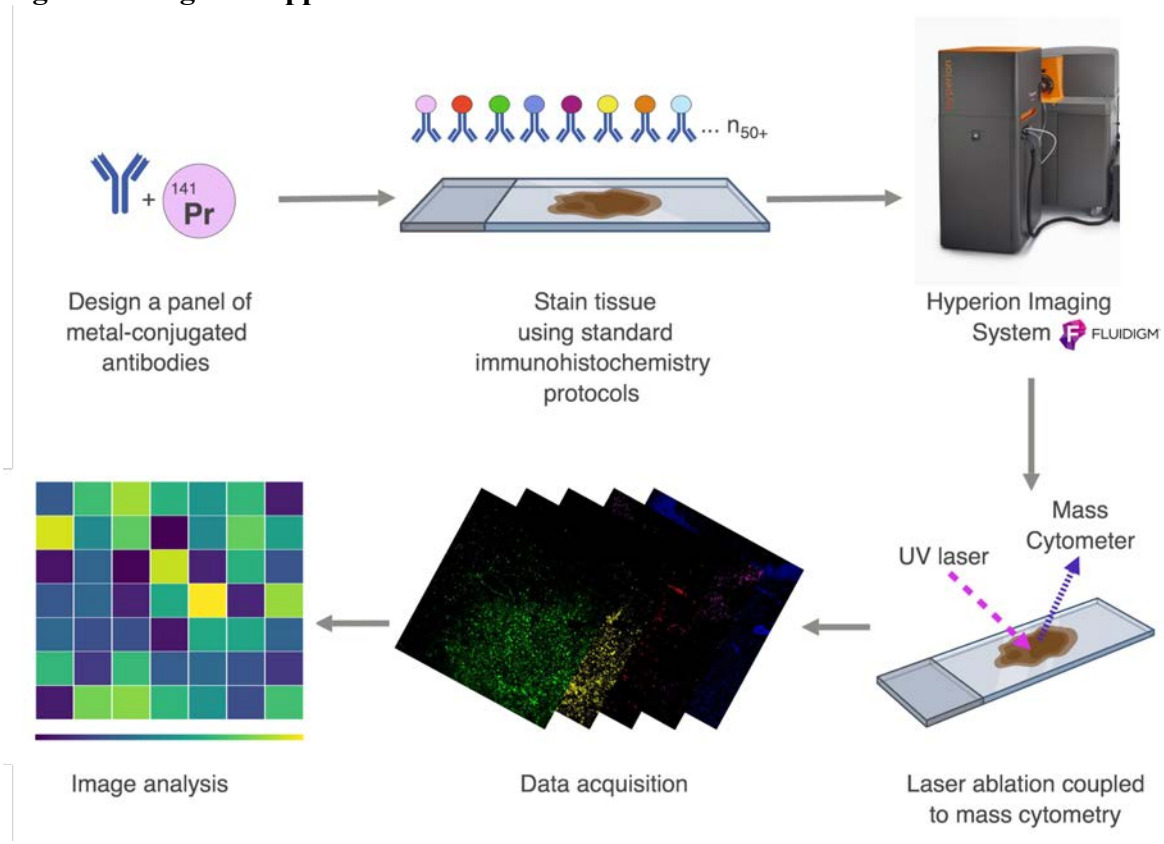

1049 **Figure 1 – Figure Supplement 3**

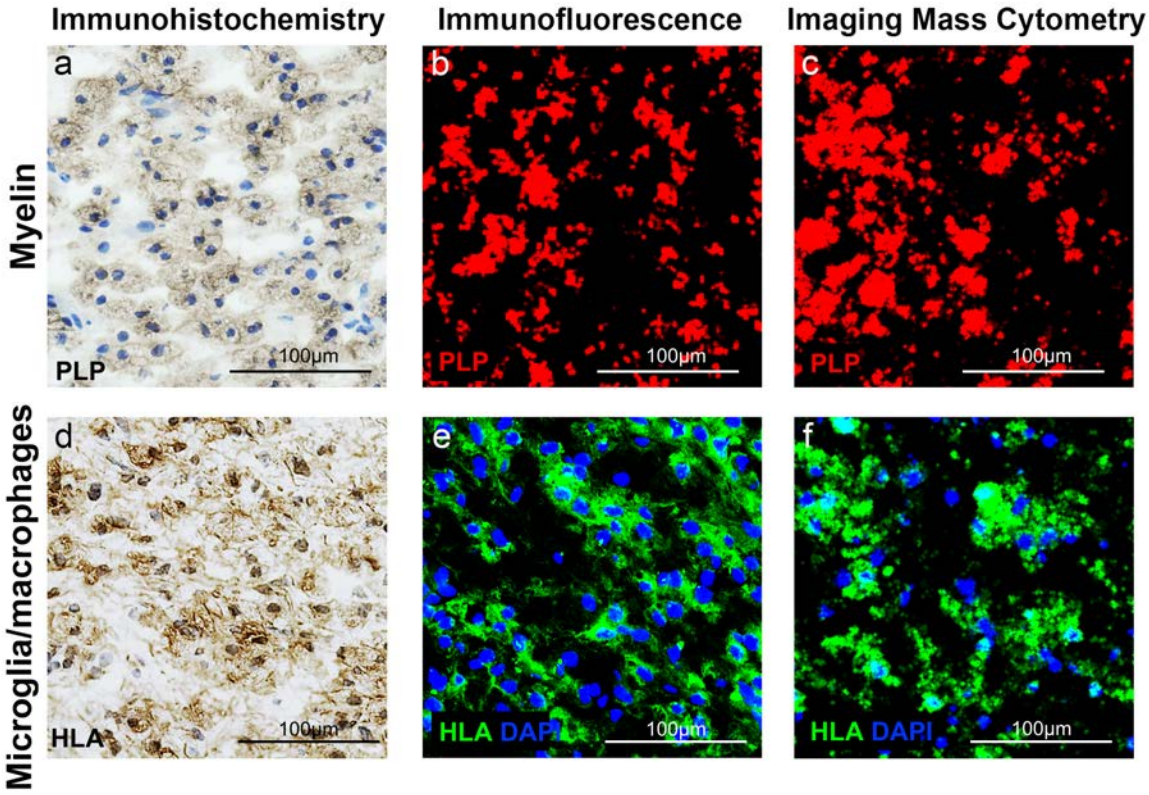

1050
1051

1052 **Figure 7 – Figure Supplement 1**

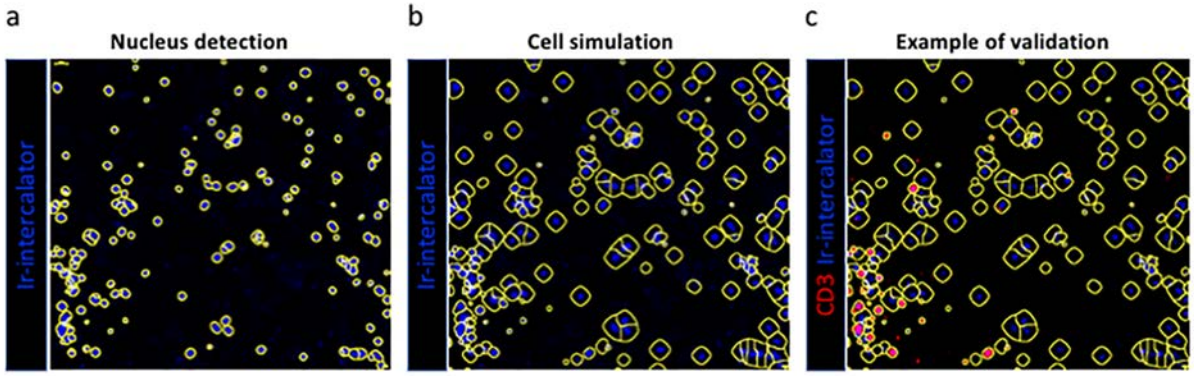

1053

1054 **Figure 7 – Figure Supplement 2**

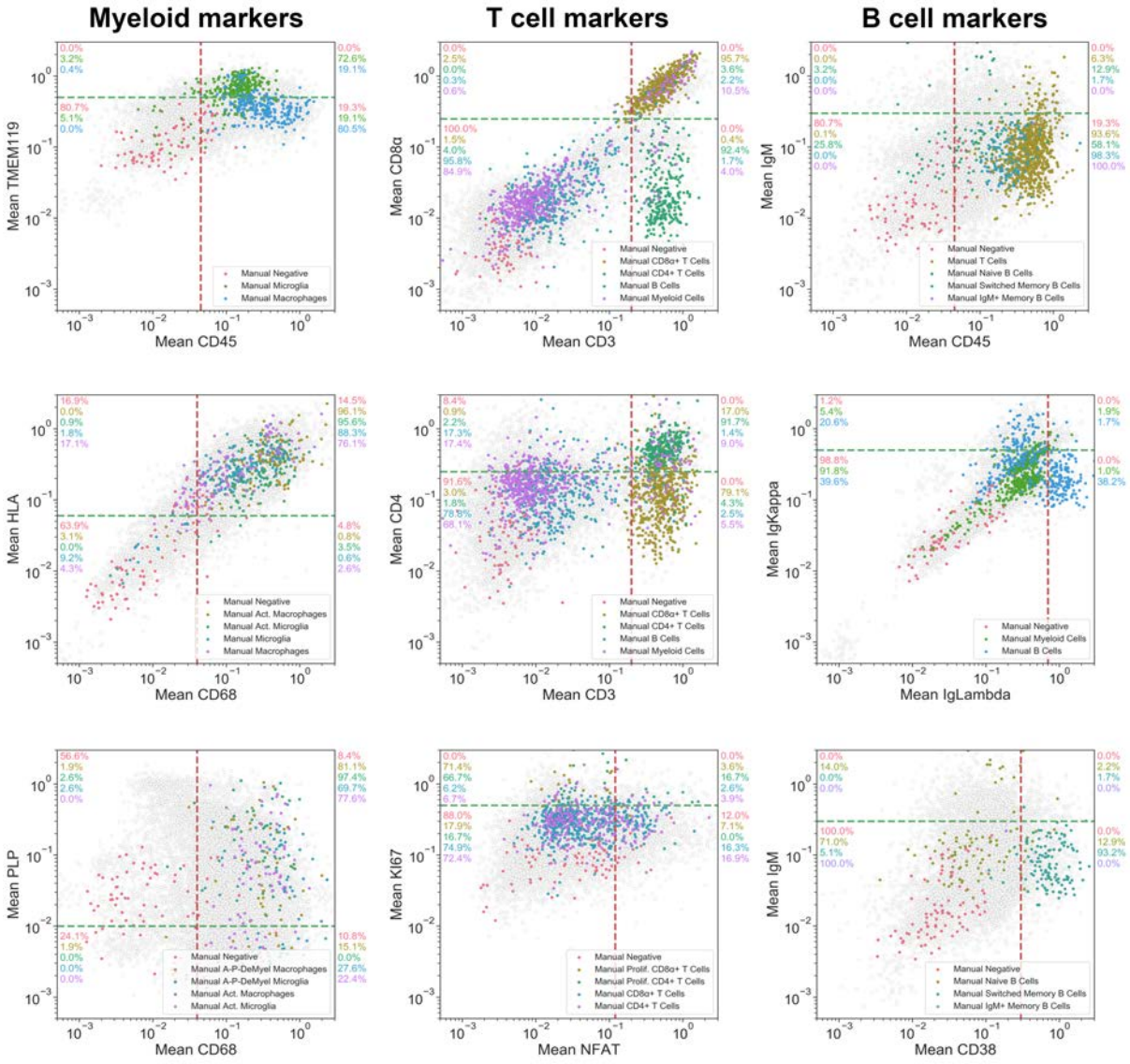

1055

1056 **Figure 7 – Figure Supplement 3**

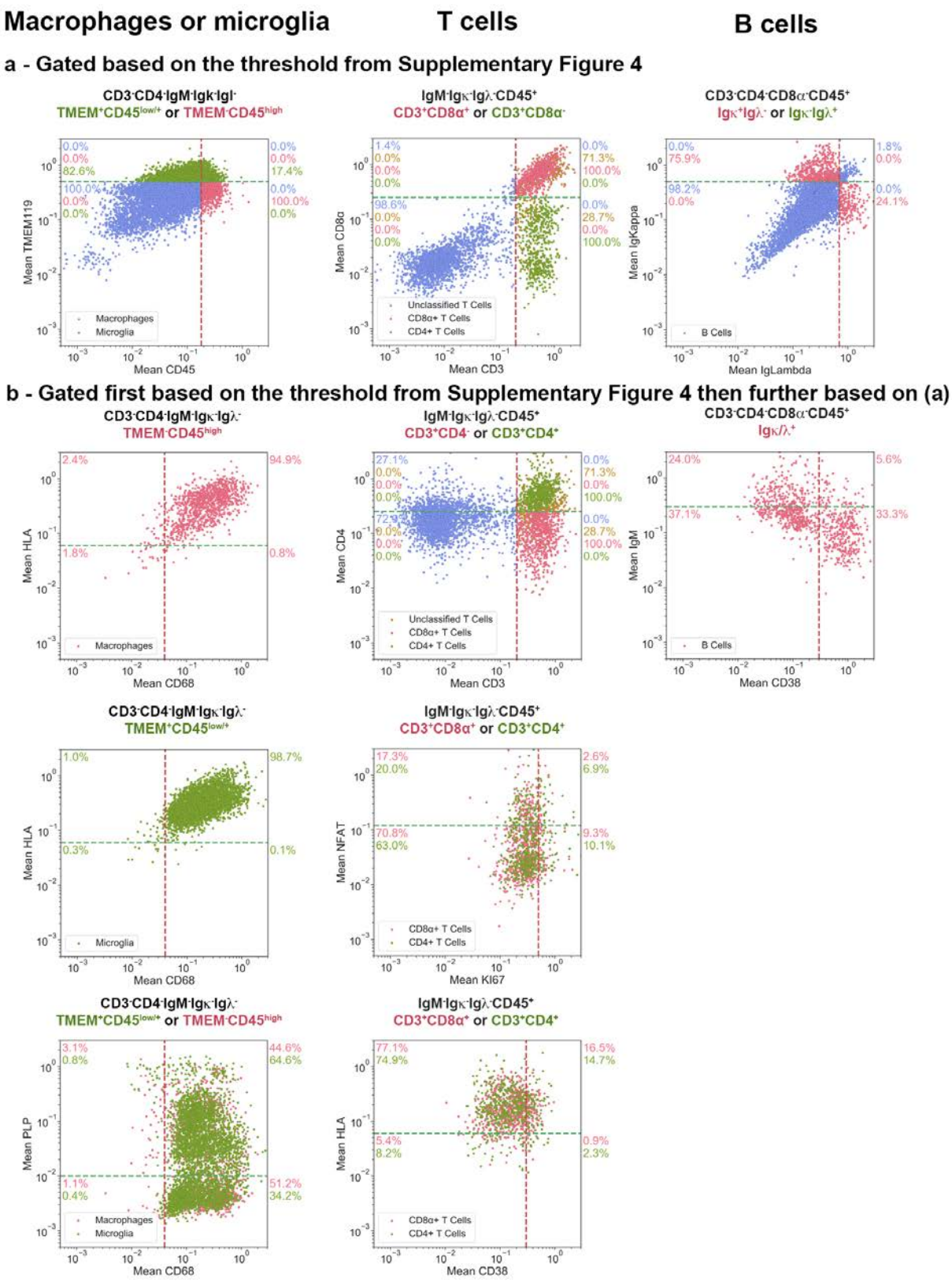

Figure 1 – Figure Supplement 1. Staging of MS lesions by IF. General pathology: demyelinating lesions (arrows and arrows head in **a** and **b**) seen in hematoxylin & eosin (HE)/Luxol fast blue (LFB) stain of myelin (**a**) and oil red o (ORO) stain of neutral lipids within macrophages (**b**). Lesional pathology: demyelinating lesions (arrow heads in **c** and **d**) visualized by proteolipid protein (PLP in red) stain of myelin (**c**) and human leukocyte antigen (HLA, in green) stain of microglia/macrophages (**d**). (**e-j**) Low magnification images of HLA and PLP stains, depicting the distribution and morphology of HLA+ microglia/macrophages and myelin in different sites and lesion stages. (**e-f**) (P)reactive lesion (block no. CR4A): Note the increase in microglia/macrophage reactivity at the (p)reactive lesion site compared to the normal-appearing white matter (NAWM) (**e**), with normal PLP myelin stain seen across the NAWM and (p)reactive lesion (**f**). (**g-h**) Active demyelinating lesion (block no. CR4A): low glia reactivity and normal myelin stain is seen in the periplaque white matter (PPWM). Profound microglia/macrophage activation is seen in the active lesion (**g**), where myelin is being destroyed (**h**). (**i-j**) Mixed active/inactive demyelinating lesion (block no. CL3A): low glia reactivity and normal myelin stain is seen in the periplaque white matter (PPWM). An increased density of HLA^+ cells with the morphology of microglia/macrophages is seen at the active SEL edge, with degraded PLP^+ myelin within macrophages (arrows head in inset). In contrast, there are only few HLA^+ cells at the inactive lesion center.

Figure 1 – Figure Supplement 2. Workflow of Imaging Mass Cytometry. A panel is designed using pathologist-verified antibodies conjugated to metals. The brain tissue is stained simultaneously with a cocktail of all the metal-conjugated antibodies and placed into the Hyperion Imaging System. The tissue is ablated by a UV laser beam ($\lambda = 219$ nm). A plume of particles produced by the laser is taken up by a flow of inert helium or argon gas and introduced

into the CyTOF mass cytometer (Hyperion Imaging System from Fluidigm (formerly DVS Sciences)). Isotopes associated with each spot are detected and indexed against the source location, yielding an intensity map of the target proteins throughout the tissue, creating spatially resolved images of multiple parameters. The acquired data is analyzed and visualized using heat maps.

Figure 1 – Figure Supplement 3. Validation of IMC staining patterns in MS lesions. Core of an active demyelinating lesion showing reduced proteolipid protein (PLP) stain by immunohistochemistry (**a**), immunofluorescence (**b**) and IMC (**c**) and corresponding areas stained with anti-HLA to detect antigen presenting cells by immunohistochemistry (**d**), immunofluorescence (**e**) and IMC (**f**).

Figure 7 – Figure Supplement 1. Single cell segmentation. A Gaussian blur was applied to the DNA signal (nucleus detection - **a**), and the resulting blurred image was segmented to identify nuclear content corresponding to individual cell areas using a combination of threshold and watershed filters (cell simulation - **b**). Subsequently, we interrogated the segmented image for the presence of specific markers or combinations of markers that are either biologically co-expressed, or whose expression is mutually exclusive. In this example we show CD3 (example of validation - **c**).

Figure 7 – Figure Supplement 2. Gating strategy used for the identification of cell subsets. Gating strategy for the identification of cell subset phenotypes and activation states of microglia, macrophages, T cells and B cells. In brief, the per-cell mean intensities of specific marker combinations are shown here in 2D log-log biaxial scatterplots. Gates were established

based on pathologist-verified positive cells (see coloured cells superimposed into each dotplot contrasting with non-verified cells in grey).

Figure 7 – Figure Supplement 3. Gating strategy used for the generation of heat maps. Using the quadrants that capture the appropriate positivity range of each cell phenotype shown in **Figure 7 – Figure Supplement 2**, cells were subjected to the positive and negative gating strategies as outlined in the Materials and Methods for each lineage and indicated in (**a**). Subsequently, these cells were plotted for the marker combinations listed in **Table 3**. The frequency of cells in each quadrant are indicated. Note that some $CD3^{+}CD45^{+}$ T cells could not be classified because they fell outside of the specified gates for either of the two markers – $CD8^{+}$ cells that were not simultaneously $CD4^{-}$, or $CD4^{+}$ cells that were not simultaneously $CD8^{-}$. This is due to the dynamic range of these particular markers and thus our inability to get a clean $CD4^{+}CD8^{-}$ or $CD4^{-}CD8^{+}$ T cell population. Cells that fulfilled the gating criteria specified above each image, but which did not fulfill the requirements for classification as Macrophages, Microglia, B cells or T cells, are shown in blue.

Source data

Figure 7 – Source Data 1

Source file for quantitative data of all ROI:

ROI 2 from block 95-056 (white matter control)

ROI 1 from block CL3a (active lesion)

ROI 2.1 from block CL3a (mixed active-inactive lesion)

ROI 2.2 from block CL3a (mixed active-inactive lesion)

ROI 3 from block CL3a (mixed active-inactive lesion)

ROI 4 from block CL3a (active lesion)

ROI 2 from block CR4a (mixed active-inactive lesion)

ROI 4 from block CR4a (active lesion)

ROI 8 from block CR4a (normal-appearing white matter)

ROI 3 from block CR4a (active lesion)

ROI 1 from block CR4a ((p)reactive lesion)

ROI 5 from block CR4a (active lesion)

ROI 6 from block CR4a (mixed active-inactive lesion)